



Contents lists available at ScienceDirect

Physica D

journal homepage: www.elsevier.com/locate/physd

Breather solutions for inhomogeneous FPU models using Birkhoff normal forms

Francisco Martínez-Farías*, Panayotis Panayotaros

Depto. Matemáticas y Mecánica, Instituto de Investigaciones en Matemáticas Aplicadas y en Sistemas, Universidad Nacional Autónoma de México, Apdo. Postal 20–726, 01000 Cd. México, Mexico

HIGHLIGHTS

- Derive inhomogeneous FPU model from elastic networks in multidimensions.
- Show examples of spatially localized normal modes in linearized FPU with spatial inhomogeneities.
- Show possibility of continuation of localized linear modes using Birkhoff normal forms.
- Compute numerically periodic orbits in quartic Birkhoff normal form, relate to spatial localization.
- Examples include localized oscillations in 3-D model with protein geometry.

ARTICLE INFO

Article history:

Received 11 January 2016
 Received in revised form
 11 May 2016
 Accepted 13 June 2016
 Available online xxxx
 Communicated by K. Josic

Keywords:

Birkhoff normal forms
 FPU lattices
 Weakly nonlinear modes
 Elastic network
 Breather solutions

ABSTRACT

We present results on spatially localized oscillations in some inhomogeneous nonlinear lattices of Fermi–Pasta–Ulam (FPU) type derived from phenomenological nonlinear elastic network models proposed to study localized protein vibrations. The main feature of the FPU lattices we consider is that the number of interacting neighbors varies from site to site, and we see numerically that this spatial inhomogeneity leads to spatially localized normal modes in the linearized problem. This property is seen in 1-D models, and in a 3-D model with a geometry obtained from protein data. The spectral analysis of these examples suggests some non-resonance assumptions that we use to show the existence of invariant subspaces of spatially localized solutions in quartic Birkhoff normal forms of the FPU systems. The invariant subspaces have an additional symmetry and this fact allows us to compute periodic orbits of the quartic normal form in a relatively simple way.

© 2016 Elsevier B.V. All rights reserved.

1. Introduction

We derive and study a class of nonlinear lattices of Fermi–Pasta–Ulam (FPU) type with a site dependent number of interacting neighbors. Our results indicate the possibility of spatially localized weakly nonlinear modes, in particular the persistence of localized linear modes that result from spatial inhomogeneities of the lattice.

The motivation comes from the question of energy localization in protein vibrations. The starting point of our analysis is the quartic nonlinear “elastic network” model of protein vibrations proposed by Juanico, Sanejouand, Piazza, and De Los Rios [1]. Elastic networks are systems of point particles interacting via spring-like forces and have been used to study vibrations of

proteins around equilibrium configurations that are considered known. The idea is to replace the complicated inter-particle potentials used in molecular dynamics by simpler, pairwise potentials that are discrete analogues of the potential energies of classical elasticity. The reference equilibrium configuration is obtained either as an equilibrium of a molecular dynamics model, or from crystallographic data for the positions of the atoms. Also, the pairwise elastic interaction only occurs between masses within a finite phenomenological interaction radius. Tirion [2] showed earlier that linear elastic networks can capture some features of low frequency protein vibration modes, while Juanico et al. [1], and Piazza and Sanejouand [3,4] added a quartic nonlinearity to the pairwise interactions and observed evidence for periodic solutions of high amplitude that are localized in regions with more pairwise interactions. The nonlinear model was justified by comparisons to molecular dynamics simulations [1]. Details of periodic orbit computations are in [3,4].

In the present paper we look for small amplitude periodic oscillations that could be continued from spatially localized normal

* Corresponding author. Fax: +55 5622 3564.

E-mail address: sairaff@ciencias.unam.mx (F. Martínez-Farías).

modes of the linearized problem. We start from two hypotheses, first that the inhomogeneous geometry of the model leads to the existence localized linear normal modes, and second that resonance arguments involving the linear frequencies and the localization properties of some normal modes can be used to construct periodic orbits in a suitable Birkhoff normal form of the system. To examine this scenario we derive an additional simplification of elastic network models by generalized quartic FPU-like systems in which every site interacts with a different number of other sites. The interactions between sites are described by a *connectivity matrix* that is determined by the geometry of the network, i.e. the positions of the masses in the equilibrium configuration, and the interaction radius of the elastic network. Our strategy is furthermore to first consider the question of localization in 1-D lattices, and then examine possible generalizations of some results obtained in these toy models to higher dimensions, especially lattices obtained from protein crystallographic data.

Starting with 1-D models, we examine oscillations around equilibrium configurations with variable density. Particles in higher density (or “agglomeration”) regions interact with more neighbors. In the simplest case where we have one such higher density region we see that the highest frequency linear normal modes are localized precisely in that region. Moreover the highest frequencies are separated from the other frequencies by a “gap”, see [5]. In the presence of more agglomeration regions we see that the gap is generally filled, while the localization of linear normal modes in the agglomeration regions persists. 3-D lattices modeling protein geometries contain several regions of higher density and can exhibit similar linear localization phenomena, without frequency gaps. In this work we study a 3-D lattice representing the protein Ribozyme.

The results on the linearized FPU lattice are in Section 2.

The frequency gaps observed in 1-D models can be used to show the existence of periodic orbits in a partial quartic Birkhoff normal form of the nonlinear system, see [5]. The periodic orbits belong to an invariant subspace of the quartic normal form that is spanned by high frequency modes that can be also spatially localized by the results of Section 2.

In the present work we generalize this argument to models without a frequency gap. To do this we examine the coefficients of quartic terms that describe the interaction between high frequency modes, and modes in a suitably defined medium frequency range. We show that the small size of these coefficients can cancel the effect of possible near-resonances and use this analysis to state a result on the existence of an invariant subspace of high frequency modes, Proposition 3, Section 3.

The calculation of periodic orbits in the invariant subspace is simplified by the fact that the restriction of the normal form to the invariant subspace has a global phase symmetry. This extra symmetry is a consequence of the small frequency width of the corresponding modes, and allows us to prove the existence of certain types of periodic orbits of “breather” type, see e.g. [6,7], using an elementary variational argument that also leads to a simple method to compute the periodic orbits numerically. Results for 1-D models and the Ribozyme are in Section 4.

In summary, the above theory is a step towards explaining spatial localization in the regions suggested by [1,3,4], but for small amplitudes. Possible extensions to high amplitudes are discussed in Section 5. Also, the paper combines theoretical statements with assumptions supported by numerics, and leaves several questions we hope to address in further work. A fully theoretical study may be possible for some 1-D models.

We note that there is an extensive literature on spectral localization at low frequencies for the homogeneous FPU lattice, see [8,9] for periodic orbits (also known as q-breathers), [10,11]

for tori. 2- and 3-D extension have been examined in [12], also for a homogeneous lattice. Results on the integrability of Birkhoff normal forms for the homogeneous 1-D FPU system in [13–15] give further information on the stability of small amplitude spectrally localized solutions. The flow of energy to higher modes can be also effectively controlled by only a few adiabatic invariants found by normal forms, see [16,13] for a related idea. Here we are concerned with the continuation of high frequency normal modes with spatial localization. In this case the mode coupling coefficients can have properties not seen in homogeneous problems (see [12] for high frequency modes of the homogeneous FPU). Numerical simulations supporting the scenario of energy localization at high frequencies will be presented elsewhere and are not directly explained by the present study. The FPU approximation and elastic network models are briefly discussed in Sections 2, and 5. We believe that the question of more general interactions should be studied further. Also, there are classical existence results on periodic orbits near elliptic equilibria, e.g. the Weinstein–Moser theorem [17,18], see also [19], the Lyapunov center theorem, see e.g. [20], and an extensive literature on periodic orbit calculations. Some relevant points are discussed in Section 5.

The paper is organized as follows. In Section 2 we present the quartic elastic model and describe the steps leading to the FPU-type model (Section 2.1). In Section 2.2 we decompose the linearized FPU system into noninteracting normal modes. Numerical examples of normal modes are shown in Section 2.3.

Section 3.1 reviews Birkhoff normal forms, explaining our notation. In Section 3.2 we discuss normal forms and invariant subspaces for lattices with frequency gaps, and in Section 3.3 we extend these arguments to cases without gap. We apply these ideas to 1-D lattices and to the Ribozyme 3-D lattice. In Section 4 we calculate some periodic orbits of breather type in the invariant subspace and check their linear stability. Examples include the Ribozyme. In Section 5 we discuss our results.

2. Localization in linearized inhomogeneous FPU lattices

In this section we seek to check our first hypothesis, namely that the spatial inhomogeneity of elastic networks used to model proteins can lead to spatially localized linear modes. A first step is to work with a somewhat simpler system, an FPU model, see Section 2.1.

In Section 2.2 we write the FPU model in normal mode variables.

The frequencies and spatial shapes of the normal modes are determined by the eigenvalues and eigenvectors of the *connectivity matrix* \mathbf{C} , defined in Section 2.2. The localization hypothesis for the linearized FPU models is checked in Section 3.3 for four examples by computing numerically and interpreting the eigenvectors of \mathbf{C} .

2.1. Derivation of FPU models from elastic networks

To define an “elastic network”, see e.g. [21,2,1], we consider a system of N point particles of mass m in \mathbb{R}^D , $D = 1, 2, 3$. The (time-dependent) position of the i th particle is denoted by \mathbf{r}_i , and we want to study motions around an equilibrium where the i th particle is at \mathbf{R}_i . We also define the relative position \mathbf{q}_i by $\mathbf{q}_i = \mathbf{r}_i - \mathbf{R}_i$ (see Fig. 1).

The potential energy we consider, see [1,4], is

$$\mathcal{U} = \sum_{i \neq j}^N c_{ij} \left[\frac{k_2}{2} (|\mathbf{r}_i - \mathbf{r}_j| - |\mathbf{R}_{ij}|)^2 + \frac{k_4}{4} (|\mathbf{r}_i - \mathbf{r}_j| - |\mathbf{R}_{ij}|)^4 \right], \quad (2.1)$$

where $\mathbf{R}_{ij} = \mathbf{R}_i - \mathbf{R}_j$, k_2 and k_4 are positive constants, and

$$c_{ij} = \begin{cases} 1 & \text{if } \mathbf{R}_{ij} \leq R_c, \\ 0 & \text{if } \mathbf{R}_{ij} > R_c, \end{cases} \quad (2.2)$$

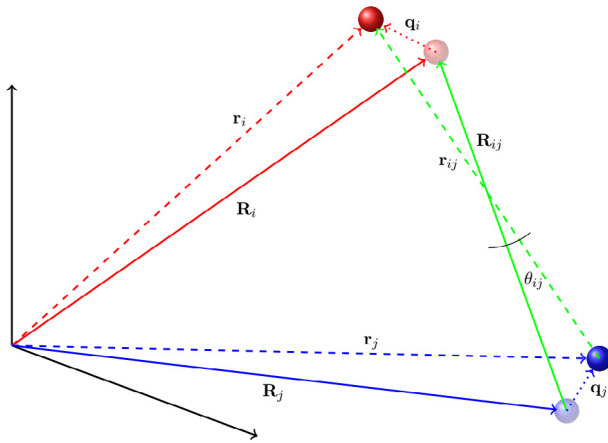


Fig. 1. Vectors \mathbf{R}_i and \mathbf{R}_j are the equilibrium positions of particles i and j respectively, while the variables \mathbf{r}_i and \mathbf{r}_j describe the positions. We also show $\mathbf{R}_{ij} = \mathbf{R}_i - \mathbf{R}_j$, $\mathbf{r}_{ij} = \mathbf{r}_i - \mathbf{r}_j$ and $\theta_{ij} = \angle(\mathbf{R}_{ij}, \mathbf{r}_{ij})$.

for some positive R_c . Also $|\cdot|$ in (2.1) denotes the Euclidean norm in \mathbb{R}^D .

The Lagrangian $\mathcal{K} - \mathcal{U}$ of the above system, \mathcal{K} the kinetic energy, \mathcal{U} as above, can be written in terms of the relative positions \mathbf{q}_i , and velocities $\dot{\mathbf{q}}_i$, and we can check that $\mathbf{q}_i = \mathbf{0}$, $\dot{\mathbf{q}}_i = \mathbf{0}$, $i = 1, \dots, N$, is a fixed point of the corresponding Euler–Lagrange equations. Thus $\mathbf{r}_i = \mathbf{R}_i$ are indeed equilibrium positions of the masses.

Taylor expansions of potentials used by molecular dynamics around a stable equilibrium will include comparable quadratic and higher order terms, however a justification of the elastic network model along these lines would require a more detailed analysis. Support for elastic network models comes from the work of Tirion [2], who adjusts k_2 , and R_c in quadratic elastic networks (i.e. \mathcal{U} as above with $k_4 = 0$) to the recover the experimental density of states of some protein vibration spectra for the lower frequency modes, see also [22,23]. The elastic network model also avoids some instabilities of molecular dynamics equilibria that are considered unphysical, see [2].

The absence of cubic terms in \mathcal{U} of (2.1) may require some further study. Piazza and Sanejouand [4] note that the exclusion of cubic terms avoids kink-like equilibria. Such solutions are indeed possible in cubic FPU models, but may be far from the origin and not as relevant to our weakly nonlinear study. It is also possible that cubic terms are nonresonant and can be eliminated. This is seen in cubic FPU lattices [13–15] and can be examined here as well.

Also, assuming that k_2 , and R_c can be estimated from experimental data, the parameter k_4 in \mathcal{U} of (2.1) characterizes the amplitude of the oscillations. For instance, it would appear in nonlinear, amplitude dependent corrections to the normal mode frequencies, but we have not seen any related experimental data.

We now make some additional assumptions to derive FPU-type models. We use the following elementary observations.

Proposition 1. Let $D = 1$ and suppose $\mathbf{R}_i > \mathbf{R}_j$ implies $\mathbf{r}_i > \mathbf{r}_j$, for all times t . Then

$$(|\mathbf{q}_i - \mathbf{q}_j + \mathbf{R}_{ij}| - |\mathbf{R}_{ij}|)^2 = |\mathbf{q}_i - \mathbf{q}_j|^2. \tag{2.3}$$

Also, let $D \geq 2$ and define

$$\theta_{ij} = \angle(\mathbf{R}_{ij}, \mathbf{r}_{ij}), \quad h = \max_{i,j=1,\dots,N} \{\theta_{ij}\}. \tag{2.4}$$

Then

$$(|\mathbf{q}_i - \mathbf{q}_j + \mathbf{R}_{ij}| - |\mathbf{R}_{ij}|)^2 = |\mathbf{q}_i - \mathbf{q}_j|^2 + O(h^2), \tag{2.5}$$

$$(|\mathbf{q}_i - \mathbf{q}_j + \mathbf{R}_{ij}| - |\mathbf{R}_{ij}|)^4 = |\mathbf{q}_i - \mathbf{q}_j|^4 + O(h^2) \tag{2.6}$$

as $h \rightarrow 0$.

Proof. The case $D = 1$ is straightforward. For $D \geq 2$, letting $\mathbf{r}_i - \mathbf{r}_j = \mathbf{q}_i - \mathbf{q}_j + \mathbf{R}_{ij}$ we have

$$\begin{aligned} (|\mathbf{q}_i - \mathbf{q}_j + \mathbf{R}_{ij}| - |\mathbf{R}_{ij}|)^2 &= |\mathbf{q}_i|^2 + |\mathbf{q}_j|^2 - 2\mathbf{q}_i \cdot \mathbf{q}_j + 2\mathbf{q}_i \cdot \mathbf{R}_{ij} \\ &\quad - 2\mathbf{q}_j \cdot \mathbf{R}_{ij} + |\mathbf{R}_{ij}|^2 \\ &\quad - 2(\mathbf{q}_i - \mathbf{q}_j + \mathbf{R}_{ij}) \cdot \mathbf{R}_{ij} \sec \theta_{ij} + |\mathbf{R}_{ij}|^2. \end{aligned}$$

Expanding the $\sec \theta_{ij}$ around $\theta_{ij} = 0$, and using (2.4) we have

$$\begin{aligned} (|\mathbf{q}_i - \mathbf{q}_j + \mathbf{R}_{ij}| - |\mathbf{R}_{ij}|)^2 &= |\mathbf{q}_i - \mathbf{q}_j|^2 + 2\mathbf{q}_i \cdot \mathbf{R}_{ij} - 2\mathbf{q}_j \cdot \mathbf{R}_{ij} \\ &\quad + |\mathbf{R}_{ij}|^2 - 2\mathbf{q}_i \cdot \mathbf{R}_{ij} + 2\mathbf{q}_j \cdot \mathbf{R}_{ij} \\ &\quad - 2|\mathbf{R}_{ij}|^2 + |\mathbf{R}_{ij}|^2 + O(h^2) \\ &= |\mathbf{q}_i - \mathbf{q}_j|^2 + O(h^2) \end{aligned}$$

as $h \rightarrow 0$. (2.6) follows similarly. \square

Considering the Hamiltonian description with $\mathbf{p}_i = m\dot{\mathbf{q}}_i$, the Hamiltonian obtained from model (2.1) in $D \geq 2$ is $\mathcal{H} + O(h^2)$, with

$$\mathcal{H} = \frac{1}{2m} \sum_{i=1}^N |\mathbf{p}_i|^2 + \sum_{i \neq j}^N c_{ij} \left[\frac{k_2}{2} |\mathbf{q}_i - \mathbf{q}_j|^2 + \frac{k_4}{4} |\mathbf{q}_i - \mathbf{q}_j|^4 \right]. \tag{2.7}$$

The second summation denotes summation over all pairs of i, j , with $i \neq j$. Model (2.7) is a generalization of the quartic FPU system, where the number of interacting neighbors is site-dependent.

2.2. Inhomogeneous FPU models in normal mode variables

The Hamiltonian \mathcal{H} of (2.7) can be written as $\mathcal{H} = \mathcal{H}_2 + \mathcal{H}_4$, with $\mathcal{H}_2, \mathcal{H}_4$ the quadratic and quartic parts of \mathcal{H} respectively. In what follows we use suitable canonical transformations to write \mathcal{H}_2 as the Hamiltonian of a system of decoupled oscillators.

We define the connectivity matrix \mathbf{C} , and the block-diagonal matrix \mathbf{C}_D , by

$$\mathbf{C} = \begin{pmatrix} n_1 & -c_{12} & \cdots & -c_{1N} \\ -c_{21} & n_2 & \ddots & \vdots \\ \vdots & \ddots & -c_{N-1N-1} & -c_{N-1N} \\ -c_{N1} & \cdots & -c_{NN-1} & n_N \end{pmatrix}, \tag{2.8}$$

$$\mathbf{C}_D = \underbrace{\begin{pmatrix} \mathbf{C} & \mathbf{0} & \cdots & \mathbf{0} \\ \mathbf{0} & \mathbf{C} & \ddots & \vdots \\ \vdots & \ddots & \mathbf{C} & \mathbf{0} \\ \mathbf{0} & \cdots & \mathbf{0} & \mathbf{C} \end{pmatrix}}_D,$$

respectively, where c_{ij} are as in (2.2), and n_i is the total number of particles interacting with the i th particle, $n_i = \sum_{j=1}^N c_{ij}$, $i = 1 \dots N$. By (2.2) we have $c_{ij} = c_{ji}$, thus \mathbf{C} , and \mathbf{C}_D are symmetric. We assume that all particles interact with at least one other particle.

Define the variables $\mathbf{p}, \mathbf{q} \in \mathbb{R}^{ND}$ as

$$\mathbf{p} = [p_{1,1}, p_{2,1}, \dots, p_{N,D}]^T, \quad \mathbf{q} = [q_{1,1}, q_{2,1}, \dots, q_{N,D}]^T, \tag{2.9}$$

where the first subscript indicates the particle index, the second the component. We can check that \mathcal{H}_2 can be written as

$$\mathcal{H}_2 = \frac{1}{2m} \langle \mathbf{p}, \mathbf{p} \rangle + k_2 \langle \mathbf{q}, \mathbf{C}_D \mathbf{q} \rangle, \tag{2.10}$$

where $\langle \cdot, \cdot \rangle$ denotes the Euclidean inner product in \mathbb{R}^{ND} . Since \mathbf{C} is symmetric we can write

$$\mathbf{C} = \mathbf{M} \mathbf{\Lambda} \mathbf{M}^T, \tag{2.11}$$

with Λ the diagonal matrix containing the real eigenvalues $\lambda_1 \leq \lambda_2 \leq \dots \leq \lambda_N$ of \mathbf{C} , and \mathbf{M} the orthogonal matrix of the eigenvectors of \mathbf{C} . Similarly,

$$\mathbf{C}_D = \mathbf{M}_D \Lambda_D \mathbf{M}_D^T,$$

where Λ_D, \mathbf{M}_D are block-diagonal, with D blocks Λ, \mathbf{M} respectively. by the nonlinear term below.

Making the symplectic change of variables

$$\mathbf{P} = \mathbf{M}_D^T \mathbf{p}, \quad \mathbf{Q} = \mathbf{M}_D^T \mathbf{q}, \tag{2.12}$$

we compute

$$\begin{aligned} \mathcal{H} = & \frac{1}{2m} \sum_{d=1}^D \sum_{l=1}^N P_{l,d}^2 + k_2 \sum_{d=1}^D \sum_{l=1}^N \lambda_l Q_{l,d}^2 \\ & + \frac{k_4}{4} \sum_{d_1, d_2=1}^D \sum_{l_1, l_2, l_3, l_4=1}^N \Gamma_{l_1 l_2 l_3 l_4} Q_{l_1, d_1} Q_{l_2, d_1} Q_{l_3, d_2} Q_{l_4, d_2}, \end{aligned} \tag{2.13}$$

with

$$\begin{aligned} \Gamma_{l_1 l_2 l_3 l_4} = & \sum_{i \neq j}^N c_{ij} (M_{i, l_1} - M_{j, l_1}) (M_{i, l_2} - M_{j, l_2}) \\ & \times (M_{i, l_3} - M_{j, l_3}) (M_{i, l_4} - M_{j, l_4}), \end{aligned} \tag{2.14}$$

where $M_{i,l}$ is the i th entry of l th column of \mathbf{M} . Note that the $\Gamma_{l_1 l_2 l_3 l_4}$ are symmetric under all permutations of the subindices.

We point out that \mathbf{C} has no negative eigenvalues, and that $\lambda_1 = 0$, in particular $\mathbf{C}\mathbf{v}_1 = \lambda_1 \mathbf{v}_1$ with $\mathbf{v}_1 = \frac{1}{N} [1, \dots, 1]^T \in \mathbb{R}^N$. We also have that $\lambda_2 > 0$, see e.g. [24] for some general facts on matrices with the structure of \mathbf{C} . The eigenvector \mathbf{v}_1 corresponds to translations of the whole system.

Then (2.14), (2.13), and $\lambda_1 = 0$ imply

$$\begin{aligned} \dot{P}_{1,d} = & -\frac{\partial \mathcal{H}}{\partial Q_{1,d}} = -\frac{k_4}{4} \frac{\partial}{\partial Q_{1,d}} \\ & \times \left\{ \sum_{d_1, d_2=1}^D \sum_{l_1, l_2, l_3, l_4=2}^N \Gamma_{l_1 l_2 l_3 l_4} Q_{l_1, d_1} Q_{l_2, d_1} Q_{l_3, d_2} Q_{l_4, d_2} \right\} \equiv 0, \end{aligned}$$

using also that by (2.14), and $\mathbf{C}\mathbf{v}_1 = 0$, we have $\Gamma_{l_1 l_2 l_3 l_4} = \dots = \Gamma_{l_1 l_2 l_3 1} = 0$.

Translational modes are eliminated by setting $P_{1,d} = 0, d = 1, \dots, D$; the Hamiltonian \mathcal{H} of (2.13) is then reduced to

$$\begin{aligned} \mathcal{H} = & \frac{1}{2m} \sum_{d=1}^D \sum_{l=2}^N P_{l,d}^2 + k_2 \sum_{d=1}^D \sum_{l=2}^N \lambda_l Q_{l,d}^2 \\ & + \frac{k_4}{4} \sum_{d_1, d_2=1}^D \sum_{l_1, l_2, l_3, l_4=2}^N \Gamma_{l_1 l_2 l_3 l_4} Q_{l_1, d_1} Q_{l_2, d_1} Q_{l_3, d_2} Q_{l_4, d_2}. \end{aligned} \tag{2.15}$$

The quadratic part of \mathcal{H} describes a set of $D(N - 1)$ decoupled harmonic oscillators, with the $N - 1$ frequencies

$$\omega_l^2 = 2 \frac{k_2 \lambda_l}{m} > 0, \quad \forall l = 2 \dots N. \tag{2.16}$$

For each $l \in \{2, \dots, N\}$ we have D components with the same frequency ω_l . By (2.13) these components are decoupled in the linear problem and are coupled by the quartic part of \mathcal{H} .

Remark 1. By $\mathbf{q} = \mathbf{M}_D \mathbf{Q}$ in (2.12), the amplitude at each site i of each of the D components of the oscillator (or mode) with frequency $\omega_l, l \in \{2, \dots, N\}$, is proportional to the i th entry of l th column $M_{i,l}$ of the matrix \mathbf{M} . “Spatial localization” of a mode l means that the amplitudes $|M_{i,l}|$ are concentrated in some small set of sites i (see the examples below).

Remark 2. The small angle assumption in Proposition 1 for $D \geq 2$ has apparently eliminated the rotational degrees of freedom.

A general formalism for small oscillations with rotational effects is discussed in [25] and references.

In Section 3 we will use the complex normal mode variables a_l, a_l^* defined by

$$\begin{aligned} \begin{pmatrix} Q'_{l,d} \\ P'_{l,d} \end{pmatrix} = & \begin{pmatrix} \sqrt{m} & 0 \\ 0 & \frac{1}{\sqrt{m}} \end{pmatrix} \begin{pmatrix} Q_{l,d} \\ P_{l,d} \end{pmatrix}, \quad \text{and} \\ a_{l,d} = & \sqrt{\frac{\omega_l}{2}} Q'_{l,d} + \frac{1}{\sqrt{2\omega_l}} P'_{l,d}, \\ a_{l,d}^* = & \sqrt{\frac{\omega_{l,d}}{2}} Q'_{l,d} - \frac{1}{\sqrt{2\omega_l}} P'_{l,d}, \end{aligned} \tag{2.17}$$

where the ω_l are as in (2.16).

Then (2.15) becomes

$$\begin{aligned} \mathcal{H} = & \sum_{d=1}^D \sum_{l=2}^N \omega_l a_{l,d} a_{l,d}^* \\ & + \frac{k_4}{4} \sum_{d_1, d_2=1}^D \sum_{l_1, l_2, l_3, l_4=2}^N \tilde{\Gamma}_{l_1 l_2 l_3 l_4} \left[a_{l_1, d_1} a_{l_2, d_1} a_{l_3, d_2} a_{l_4, d_2} \right. \\ & + 4a_{l_1, d_1} a_{l_2, d_1} a_{l_3, d_2} a_{l_4, d_2}^* + 6a_{l_1, d_1} a_{l_2, d_1} a_{l_3, d_2}^* a_{l_4, d_2}^* \\ & \left. + 4a_{l_1, d_1} a_{l_2, d_1}^* a_{l_3, d_2}^* a_{l_4, d_2}^* + a_{l_1, d_1}^* a_{l_2, d_1}^* a_{l_3, d_2}^* a_{l_4, d_2}^* \right], \end{aligned} \tag{2.18}$$

with

$$\tilde{\Gamma}_{l_1 l_2 l_3 l_4} = \frac{\Gamma_{l_1 l_2 l_3 l_4}}{4m^2 \sqrt{\omega_{l_1} \omega_{l_2} \omega_{l_3} \omega_{l_4}}}. \tag{2.19}$$

Hamilton’s equations become

$$\dot{a}_{l,d} = -i \frac{\partial \mathcal{H}}{\partial a_{l,d}^*}, \quad l \in \{2, \dots, N\}, \quad d \in \{1, \dots, D\}. \tag{2.20}$$

Remark 3. The numerical studies below suggest that the frequencies ω_l for the smallest indices l in (2.19) can reach small values and vanish in the limit of infinite particles. The coefficients $\Gamma_{l_1 l_2 l_3 l_4}$ however decrease at a comparable rate and the coefficients $\tilde{\Gamma}_{l_1 l_2 l_3 l_4}$ do not grow. This fact is seen explicitly in the lattice with nearest neighbor interactions, see e.g. [5,13,12].

2.3. Spectral analysis of the connectivity matrix

In what follows we present some numerical results on the spectra and eigenvalues of the connectivity matrix \mathbf{C} of some 1-D and 3-D configurations. The 3-D example is constructed using crystallographic data for the protein Ribozyme. Our plan is to first examine some 1-D examples and identify features that can be partially generalized to 3-D protein examples. The numerical linear algebra computations below were performed using the GSL libraries [26].

In 1-D we consider configurations where the equilibrium positions \mathbf{R}_i of most particles are equidistant, and examine the effect of introducing one or more “agglomeration” regions where the \mathbf{R}_i are more dense. These regions correspond to sites that interact with more neighbors. We see that agglomeration regions can introduce gaps in the spectrum, and also lead to spatially localized normal modes. Examples 1–3 indicate variants of this scenario, while Example 4 shows results for the 3-D protein example, see also Table 1.

The linear spectrum of the different configurations is visualized in Figs. 3(a), 5(a), 7(a), and 8(b) by plotting the “dispersion

Table 1
Examples of lattices.

Example	Number of particles N	Dimension	Number of agglomeration regions
(1)	113	1	1
(2)	113	1	2
(3)	113	1	3
(4)	879	3	NA

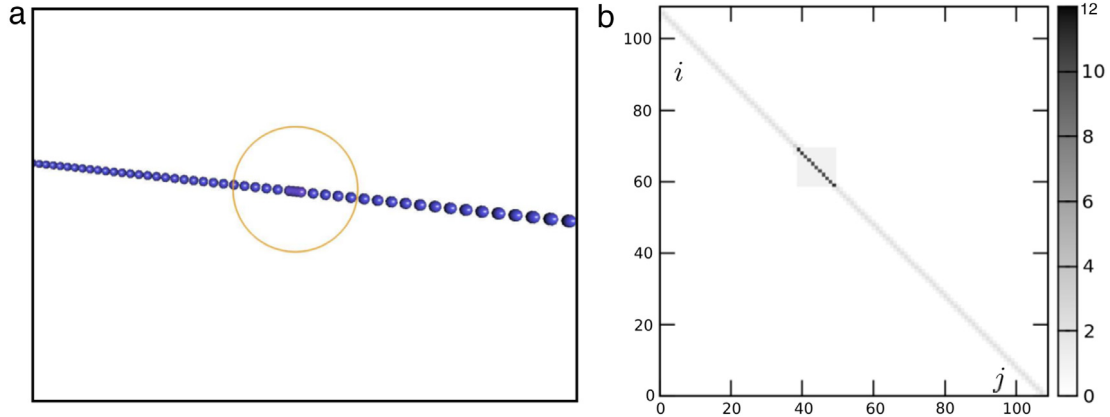


Fig. 2. Example 1: (a) 1-D chain with one agglomeration zone (circled). (b) Graphic representation of the connectivity matrix C , $i, j \in \{1, \dots, N\}$, $N = 113$. The agglomeration region corresponds to the block with larger values in the diagonal.

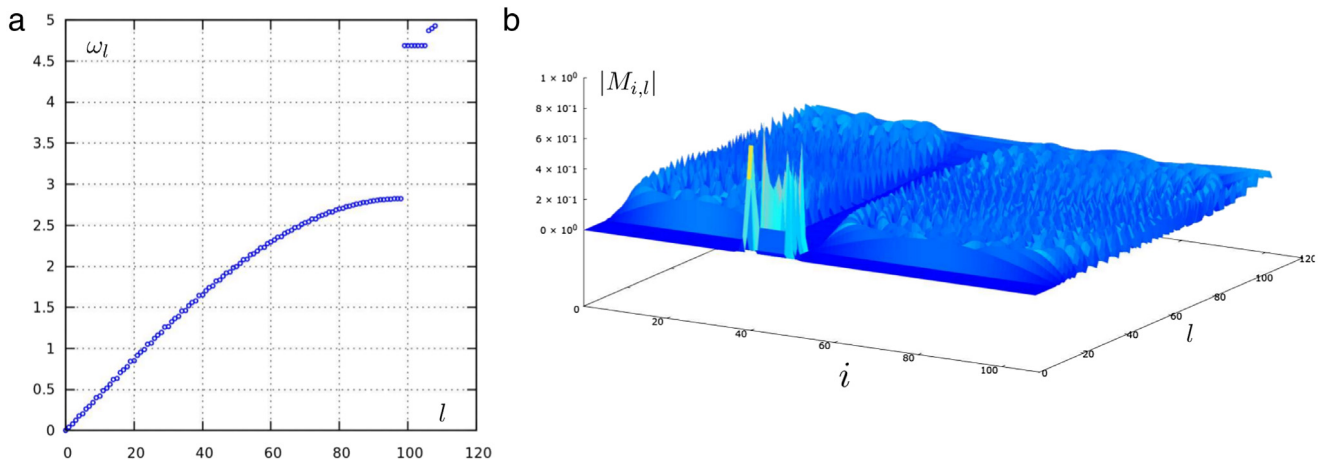


Fig. 3. Example 1: (a) Frequency ω_l vs. wavenumber l , (b) Plot of eigenmodes: absolute value $|M_{i,l}|$ of $M_{i,l} = i$ th entry of l th eigenvector, $i \in \{1, \dots, N\}$, $l \in \{2, \dots, N\}$, $N = 113$. Localization of the high frequency modes is indicated by the spikes in the region of high l , and of i in the agglomeration region.

relation" ω_l vs. l , where the generalized "wavenumber" l is an index enumerating the frequencies in increasing order. In $D \geq 2$ models with symmetries, e.g. a two dimensional hexagonal lattice, it may be possible to use vectors of indices instead, but this does not seem applicable in the 3-D example considered here.

Eigenfunctions of 1-D models are visualized in Figs. 3(b), 5(b), 7(b) by plotting the absolute value of the entries of the matrix of eigenvalues \mathbf{M} vs. indices l, i : the entry $M_{i,l}$ is the value of the l th eigenvector of \mathbf{C} at site i , where l enumerates the eigenvalues in increasing order.

Example 1. $D = 1, N = 113$: This chain has one agglomeration region of about 10 particles, indicated in Fig. 2(a). R_c is chosen so that most particles interact with two neighbors. This leads to a connectivity matrix that is mostly tridiagonal, with a larger block corresponding to the agglomeration region, see Fig. 2(b). The larger diagonal elements in that block indicate the larger number of interactions among the sites in the agglomeration region. Fig. 3(a) indicates a gap between a set of "low" and "high" frequencies, moreover Fig. 3(b) indicates that the normal modes

corresponding to the high frequencies are localized in the sites of the agglomeration region. Specifically, we see that if $l \geq 99$ we have $|M_{i,l}| < 10^{-5}$ for all $i \notin \{40, \dots, 50\}$.

The following two examples show that the presence of more agglomeration regions can introduce frequencies that start to fill the frequency gap seen in the first example. Nevertheless the localization of the normal modes in the agglomeration regions persists.

Example 2. $D = 1, N = 113$: This chain has two agglomeration regions, see Fig. 4(a), and two larger blocks in its connectivity matrix, see Fig. 4(b). The dispersion relation in Fig. 5(a) indicates smaller gaps between more regions of frequencies, i.e. "low", "middle", and "high" frequencies. Alternatively we may say that the large gap seen in Example 1 is "filled" by intermediate frequencies. Fig. 5(b) shows that the highest frequency normal modes are strongly localized in the sites of the two agglomeration regions. Moreover the overlap of the modes localized in each agglomeration region is negligible. In particular, we see that if $l \geq 104$ then $|M_{i,l}| < 10^{-5}$ for all $i \notin \{40, \dots, 45\} \cup \{83, \dots, 94\}$.

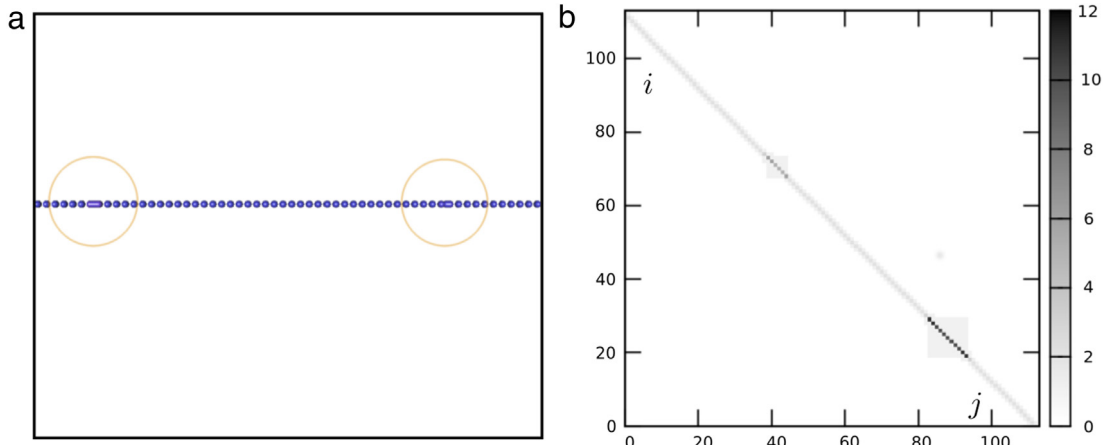


Fig. 4. Example 2: (a) 1-D chain with two agglomeration zones (circled), (b) Graphic representation of connectivity matrix C , $i, j \in \{1, \dots, N\}$, $N = 113$. The two agglomeration regions correspond to two blocks with larger values in the diagonal.

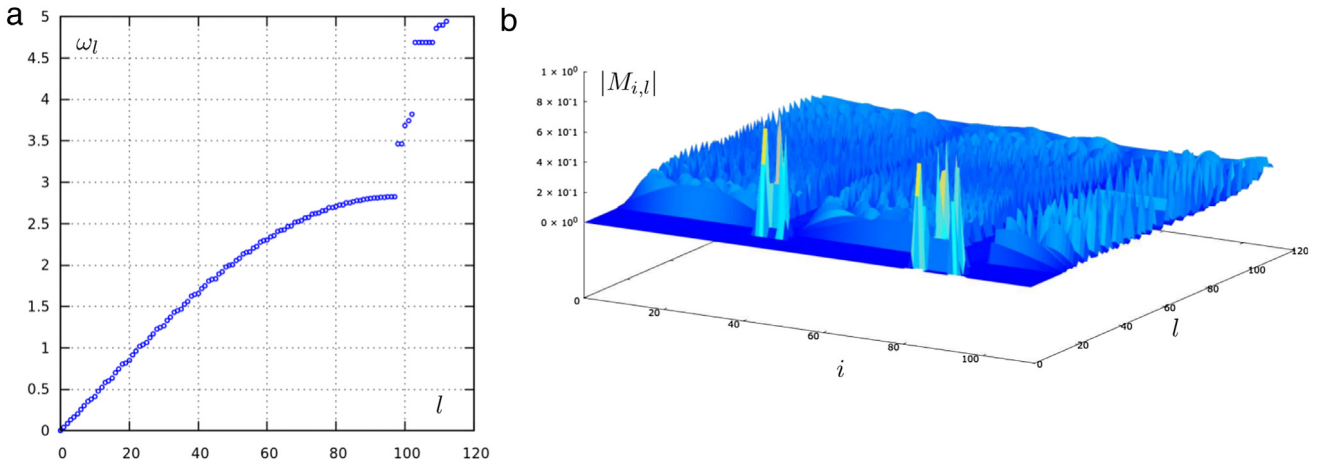


Fig. 5. Example 2: (a) Frequency ω_l vs. wavenumber l . (b) Plot of eigenmodes: $M_{i,l} =$ i th entry of l th eigenvector, $i \in \{1, \dots, N\}$, $l \in \{2, \dots, N\}$, $N = 113$. Localization of the high frequency modes is indicated by the spikes in the region of high l , and of i in the two agglomeration regions.

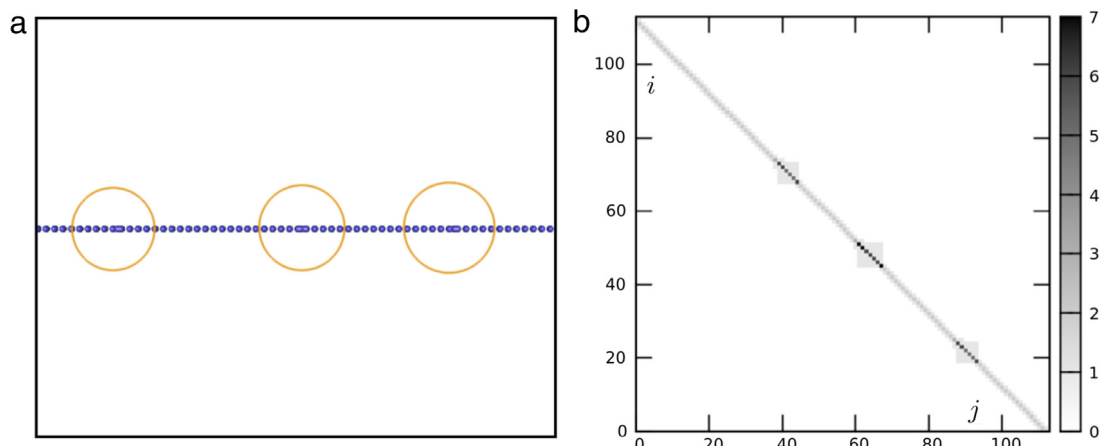


Fig. 6. Example 3: (a) 1-D chain with three agglomeration zones (circled), (b) Graphic representation of connectivity matrix C , $i, j \in \{1, \dots, N\}$, $N = 113$. The three agglomeration regions correspond to three blocks with larger values in the diagonal.

Example 3. $D = 1$, $N = 113$: This chain has three agglomeration regions, see Fig. 6(a), and three larger blocks in its connectivity matrix, see Fig. 6(b). The dispersion relation in Fig. 7(a) indicates more frequencies filling the gap of Example 1. Fig. 7(b) indicates the existence of several strongly localized high frequency modes. The modes are localized in the agglomeration regions, i.e. we see that if

$$l \geq 102 \text{ then } |M_{i,l}| < 10^{-5} \text{ for all } i \notin \{40, \dots, 44\} \cup \{62, \dots, 68\} \cup \{89, \dots, 95\}.$$

Example 4. $D = 3$, $N = 879$: The equilibrium positions \mathbf{R}_i are now vectors in \mathbb{R}^3 and correspond to the positions of the atoms of the protein Ribozyme, as obtained by Scott and James, see [27], using

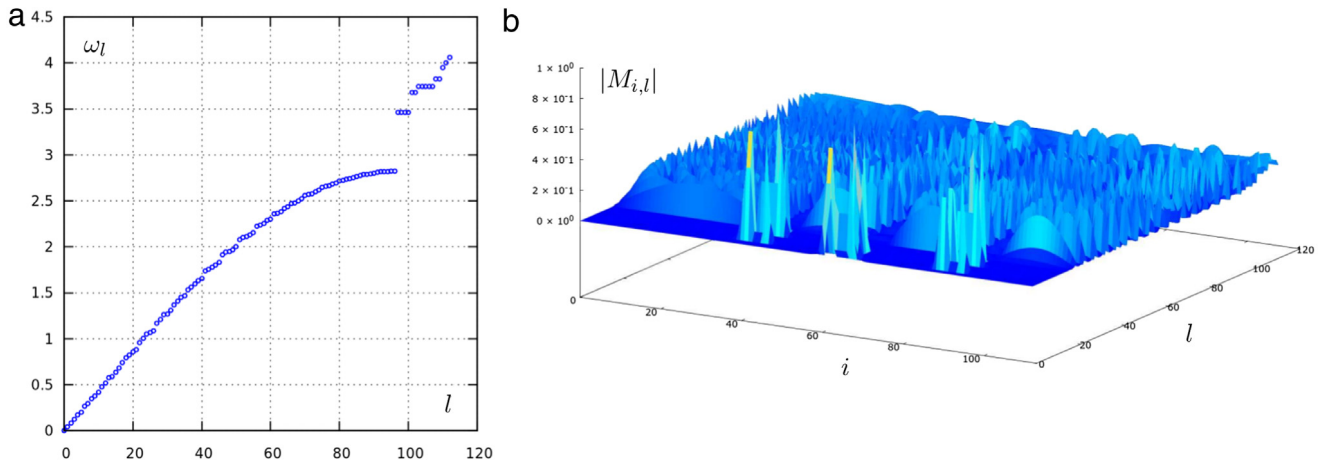


Fig. 7. Example 3: (a) Frequency ω_l vs. wavenumber l , (b) Plot of eigenmodes: $M_{i,l}$ = i th entry of l th eigenvector, $i \in \{1, \dots, N\}$, $l \in \{2, \dots, N\}$, $N = 113$. Localization of the high frequency modes is indicated by the spikes in the region of high l , and of i in the two agglomeration regions.

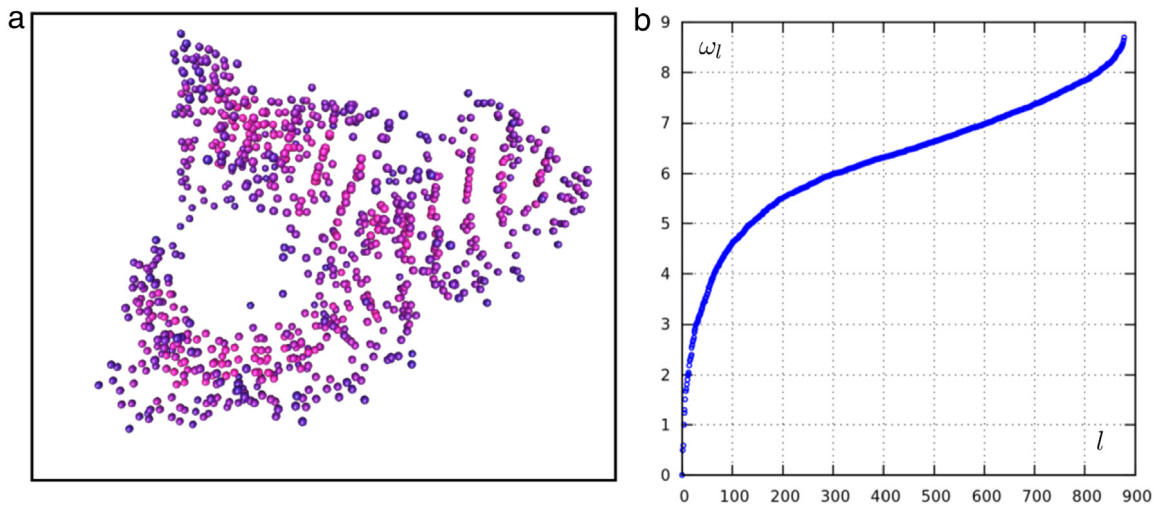


Fig. 8. Example 4: (a) Projection of 3-D plot of atom locations \mathbf{R}_i for Ribozyme (PDB300), \mathbf{R}_i obtained from crystallographic measurements, (b) Frequency ω_l vs. “wavenumber” index l , $l \in \{2, \dots, N\}$, $N = 879$.

crystallography techniques. These data are publicly available and were downloaded from the database [28]. The positions \mathbf{R}_i of the atoms are indicated in Fig. 8(a). The Ribozyme is sometimes called “Hammerhead” due to its shape.

The connectivity matrix \mathbf{C} depends on the choice of R_c , and we have chosen here $R_c = 4.5 \text{ \AA}$ ($1 \text{ \AA} = 10^{-10} \text{ m}$). Also, following [22], we consider only the carbon atoms in the protein. The choice of R_c is discussed by many authors. It must be large enough so that all particles have at least one neighbor, but it is argued that if R_c is too large then relevant smaller scale features are not captured correctly. In particular, [23] argues that we should use $R_c \leq 7 \text{ \AA}$ for the Ribozyme, while [22] uses $R_c = 5 \text{ \AA}$.

Fig. 8(b) shows that there are no gaps in the spectrum. In Fig. 9 we visualize two normal modes for different frequency ranges. Fig. 9(b) shows an example of strong spatial localization in the highest frequency range. An indication of spatial localization is the fact that for $l \geq 850$ we have $|M_{i,l}| < 10^{-3}$ for all i outside a set of 22 sites.

In the next section we examine the question of whether the localized modes seen above can be continued to the weakly nonlinear regime.

3. Birkhoff normal form and approximate invariant subspaces

In this section we use Birkhoff normal forms, see e.g. [20], to remove some nonresonant quartic terms in the Hamiltonian so

that the remaining quartic normal form systems have invariant subspaces of high frequency modes. These modes are spatially localized in the sense of the previous section. In Section 3.1 we recall some basic facts about Birkhoff normal forms and resonances in the context of our problem. In Section 3.2 we describe the invariant subspace argument for lattices with a gap in the spectrum, see Proposition 2.

In Section 3.2 we generalize to cases without frequency gap, examining the coefficients of certain interactions between modes in suitably defined high and medium frequency ranges for Examples 2–4 of the previous section. The existence of the invariant subspace is stated as Proposition 3.

3.1. Birkhoff normal forms and resonances

The Birkhoff normal form method aims to simplify a Hamiltonian $\mathcal{H}(z)$ around the origin by a symplectic change of variables. To outline the main step, let $z, w \in \mathbb{R}^{2n}$, where w represents the new variables. Consider a symplectic change of variable $z = f_1(w)$, where f_s is the time- s map of the system

$$\frac{d}{ds} w(s) = \mathbb{J} \nabla \mathcal{H}(w(s)), \tag{3.1}$$

with $w(0) = w$ and $z = w(1) = f_1(w)$. \mathbb{J} is the symplectic matrix in \mathbb{R}^{2n} . The Hamiltonian in the variables z, w satisfies $\mathcal{H}(z) =$

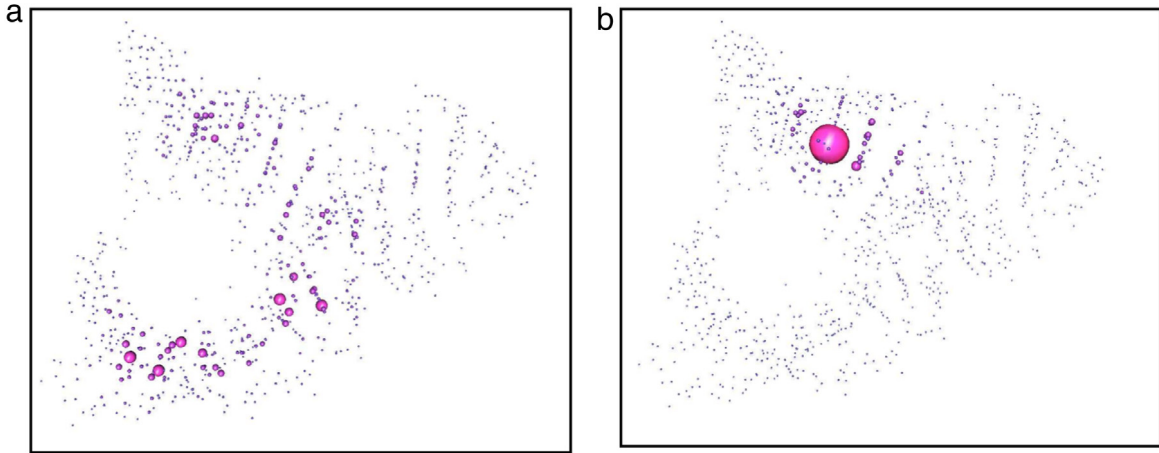


Fig. 9. Example 4: Amplitude localization of some eigenfunctions of Ribozyme for (a) $l = 800$, (b) $l = 879$ (highest frequency mode). In all cases the radius of the ball centered at \mathbf{R}_i represents the absolute value of the eigenfunction at the site i .

$\mathcal{H}(f_1(w)) = (\mathcal{H} \circ f_1)(w)$, and we also have

$$\begin{aligned} \frac{d}{ds}(\mathcal{H} \circ f_s)(w) &= [\nabla \mathcal{H}(w(s))]^T \frac{dw(s)}{ds} \\ &= [\nabla \mathcal{H}(w(s))]^T \mathbb{J} \nabla \mathcal{S}(w(s)) = [\mathcal{H}, \mathcal{S}](w(s)), \end{aligned} \quad (3.2)$$

using the definition of the Poisson bracket. Similarly, the higher derivatives are

$$\frac{d^n}{ds^n} \mathcal{H}(w(s)) = \underbrace{[\dots [\mathcal{H}, \mathcal{S}], \mathcal{S} \dots \mathcal{S}]}_{n \text{ times}} w(s), \quad n = 1, 2, \dots \quad (3.3)$$

Combining (3.3) and the Taylor expansion of the Hamiltonian $\mathcal{H}(w(s))$ around $s = 0$ we have

$$\begin{aligned} \mathcal{H}(w(s)) &= \mathcal{H}(w(0)) + s[\mathcal{H}, \mathcal{S}](w(0)) \\ &\quad + \frac{1}{2}s^2[[\mathcal{H}, \mathcal{S}], \mathcal{S}]w(0) + \dots, \quad \forall s \in [0, 1], \end{aligned} \quad (3.4)$$

assuming convergence of the series (3.4), $\forall s \in [0, 1]$. In particular, for $s = 1$, (3.4) becomes

$$\mathcal{H}(z) = \mathcal{H}(w) + [\mathcal{H}, \mathcal{S}](w) + \frac{1}{2}[[\mathcal{H}, \mathcal{S}], \mathcal{S}](w) + \dots \quad (3.5)$$

The left hand side then gives us an explicit expression of the Hamiltonian in the new variables w , and the general idea is to choose \mathcal{S} so as to simplify the right hand side, in a sense that depends on the problem, see below for the present case. The procedure can be also iterated.

For the case where \mathcal{H}, \mathcal{S} are real analytic, the infinite series (3.4) converges sufficiently near the origin, see e.g. [29,30], i.e. within a ball of radius ρ in the variable w . Moreover, the change of variables $z = f_1(w)$ is given explicitly (as a power series) and has the form $z = w + g_s(w)$, where g_s vanishes as $w \rightarrow 0$, i.e. the change of coordinates is a small perturbation of the identity near the origin.

In the present case we write the Hamiltonian \mathcal{H} of (2.18) in the original variables $z = (\tilde{a}, \tilde{a}^*)$, $\tilde{a} = (\tilde{a}_{1,1}, \dots, \tilde{a}_{N,D})$, i.e. we use $\tilde{a}_{i,d}$ instead of $a_{i,d}$, as

$$\mathcal{H}(z) = \mathcal{H}_2(z) + \mathcal{H}_4(z), \quad (3.6)$$

where \mathcal{H}_2 and \mathcal{H}_4 are the quadratic and quartic terms respectively of (2.18). We will use a symplectic change of coordinates as described above to eliminate some of the (quartic) monomials \mathcal{H}_4 , up to higher order terms.

Let \mathcal{S} be the sum of the quartic monomials $\mathcal{S}_{\mathcal{M}}$

$$\mathcal{S} = \sum_{\mathcal{M} \in \mathcal{J}} \mathcal{S}_{\mathcal{M}}, \quad (3.7)$$

where \mathcal{J} is the set of quartic monomials of \mathcal{H}_4 we want to eliminate.

Then, (3.5) and the properties of the Poisson bracket imply

$$\begin{aligned} \mathcal{H}(z) &= \mathcal{H}(w) + [\mathcal{H}, \mathcal{S}](w) + O(6), \\ &= \mathcal{H}_2(w) + [\mathcal{H}_2, \mathcal{S}](w) + \mathcal{H}_4(w) + O(6), \end{aligned} \quad (3.8)$$

$$= \mathcal{H}_2(w) + \tilde{\mathcal{H}}_4(w) + O(6), \quad (3.9)$$

where $O(6)$ means terms of degree six or higher in the (new) variables $w = (a, a^*)$, $a = (a_{1,1}, \dots, a_{N,D})$, and $\tilde{\mathcal{H}}_4 = [\mathcal{H}_2, \mathcal{S}](w) + \mathcal{H}_4(w)$.

We also define the quartic normal form Hamiltonian $\tilde{\mathcal{H}}$ as

$$\tilde{\mathcal{H}} = \mathcal{H}_2 + \tilde{\mathcal{H}}_4. \quad (3.10)$$

The system described by the Hamiltonian $\tilde{\mathcal{H}}$ is considered an approximation of the full system on the right hand side of (3.9), see comments at the end of the subsection, and is a simplification of the original system of \mathcal{H} in the sense that $\tilde{\mathcal{H}}_4$ has fewer quartic monomials than \mathcal{H}_4 . Some consequences of this fact are seen in the following subsections.

To see what quartic monomials of \mathcal{H}_4 can be eliminated, note that by (3.8), a quartic monomial \mathcal{M} in \mathcal{H}_4 is eliminated by a quartic monomial $\mathcal{S}_{\mathcal{M}}$ in (3.7) that satisfies

$$[\mathcal{H}_2, \mathcal{S}_{\mathcal{M}}] + \mathcal{M} = 0. \quad (3.11)$$

We see that to eliminate $\mathcal{M} = \tilde{\Gamma}_{k_1 k_2 k_3 k_4} b_{k_1, d_1} b_{k_2, d_2} b_{k_3, d_3} b_{k_4, d_4}$ in \mathcal{H}_4 , with $b_{k_j, d_j} = a_{k_j, d_j}$, or a_{k_j, d_j}^* , we must choose

$$\mathcal{S}_{\mathcal{M}} = \frac{i \tilde{\Gamma}_{k_1 k_2 k_3 k_4}}{\sum_i \sigma(k_i) \omega_{k_i}} b_{k_1} b_{k_2} b_{k_3} b_{k_4}, \quad (3.12)$$

where $\sigma(k_i) = 1$ if $b_{k_i, d_i} = a_{k_i, d_i}$, -1 if $b_{k_i, d_i} = a_{k_i, d_i}^*$. Quartic monomials for which $\sum_{j=1}^4 \sigma(k_j) \omega_{k_j} = 0$ (and $\tilde{\Gamma}_{k_1 k_2 k_3 k_4} \neq 0$) are called resonant. The resonant monomials cannot be eliminated by the above procedure.

While all non-resonant monomials can be eliminated by a symplectic transform defined in some ball of radius ρ around the origin, the size of ρ is controlled by \mathcal{S} , and the coefficients of the monomials (3.12), see e.g. [29,30]. In Sections 3.2, 3.3 we eliminate non-resonant quartic monomials using terms $\mathcal{S}_{\mathcal{M}}$ whose coefficients that are below certain bounds. These bounds can be then used to estimate ρ . This will be pursued in further work.

The approximation of solutions of the FPU system with Hamiltonian \mathcal{H} by solutions of the system with the Hamiltonian $\tilde{\mathcal{H}}$ of (3.10), i.e. the normal form system, is heuristic at this point.

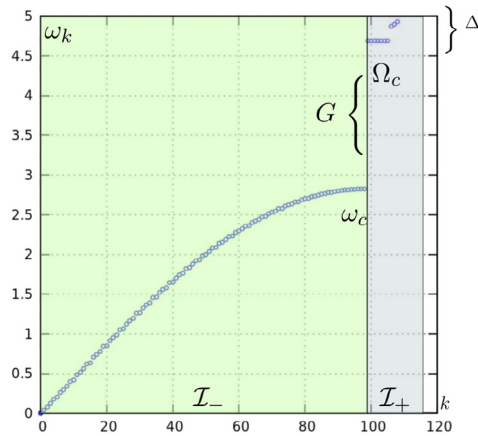


Fig. 10. Example of gap between low frequency modes \mathcal{I}_- and high frequency \mathcal{I}_+ modes (taken from Example 1).

The rough idea is that for small enough initial conditions i.e. within a ball of radius ρ around the origin, the term $O(6)$ in (3.9) is a small perturbation of the normal form system, so that the solutions of the normal form system are ϵ -near the solutions of the full system, for times of order ϵ^{-1} . Such a result generally holds as $\rho \sim \epsilon$ vanishes, see e.g. [29,30]. A more precise quantitative statement of this type, relating ρ, ϵ with the parameters of each lattice, is outside the scope of this paper, but again the bounds on the coefficients of the monomials (3.12) in Sections 3.2, 3.3 are a first step towards such a theory. We comment further on these issues in the next subsections, and in Section 5.

3.2. Invariant subspaces: cases with frequency gap

We now apply the Birkhoff normal form procedure to eliminate certain quartic monomials of \mathcal{H}_4 by assuming a gap between the frequencies of the quadratic term \mathcal{H}_2 . This scenario is indicated in Fig. 10, and is motivated by Example 1 of the previous section. Since this gap is seen in a 1-D example, we will assume here that we are studying a 1-D lattice. We will need only the subindex l for the variables $a_{l,1}$, and we let $a_l = a_{l,1}, l \in \{2, \dots, N\}$.

We separate the modes into two sets \mathcal{I}_- and \mathcal{I}_+ that are below and above the gap respectively. We will make the following assumptions on the frequencies: consider disjoint sets $\mathcal{I}_-, \mathcal{I}_+$ satisfying $\mathcal{I}_- \cup \mathcal{I}_+ = \{2, \dots, N\}$, so that letting

$$\omega_c = \max_{j \in \mathcal{I}_-}(\omega_j), \quad \Omega_c = \min_{j \in \mathcal{I}_+}(\omega_j), \quad (3.13)$$

we have $\omega_c < \Omega_c$. Also let

$$G = \Omega_c - \omega_c, \quad \Delta = \max_{i,j \in \mathcal{I}_+} |\omega_i - \omega_j|, \quad i, j \in \mathcal{I}_+, \quad (3.14)$$

and assume

$$\Omega_c - \Delta \geq O(1), \quad G \geq O(1), \quad G - \Delta \geq O(1). \quad (3.15)$$

The notation $O(1)$ assumes that there is a small parameter in the problem. A possible small parameter here is the smallest frequency ω_2 of the chain (alternatively the inverse of the size of the chain N^{-1}), so that $O(1)$ means independent of ω_2 (or N^{-1}).

This notion becomes well defined when the chains of Examples 1–3 are extended to arbitrary size from both sides, with nearest neighbor interactions in the extensions. $O(1)$ quantities are the ones that are expected to approach a nonzero constant in the limit.

We now show the existence of a quartic normal form with an invariant subspace.

Table 2
Monomials in the equations of motion and their origin in the Hamiltonian.

Case	Monomial in $\dot{a}_k, k \in \mathcal{I}_{k_1, k_2, k_3} \in \mathcal{I}_+$	Monomial in quartic Hamiltonian
(1)	$a_{k_1} a_{k_2} a_{k_3}$	$a_{k_1} a_{k_2} a_{k_3} a_{k_4}^*$
(2)	$a_{k_1} a_{k_2} a_{k_3}^*$	$a_{k_1} a_{k_2} a_{k_3}^* a_k^*$
(3)	$a_{k_1} a_{k_2}^* a_{k_3}^*$	$a_{k_1} a_{k_2}^* a_{k_3}^* a_k^*$
(4)	$a_{k_1} a_{k_2} a_{k_3}^*$	$a_{k_1} a_{k_2} a_{k_3}^* a_{k_4}^*$
(5)	$a_{k_1} a_{k_2}^* a_{k_3}^*$	$a_{k_1} a_{k_2}^* a_{k_3}^* a_{k_4}^*$
(6)	$a_{k_1} a_{k_3}^* a_{k_2}^*$	$a_{k_1} a_{k_3}^* a_{k_2}^* a_{k_4}^*$

Table 3
Frequency sums for quartic monomials of degree 3 in the variables $a_k, a_k^*, k \in \mathcal{I}_-$, and degree 1 in the variables $a_k, a_k^*, k \in \mathcal{I}_+$. (Numbers are those of Table 1.)

Case	Frequency sum denominator
(1)	$\Omega_{l_1} + \Omega_{l_2} + \Omega_{l_3} - \tilde{\omega}_{l_4} \geq \Omega_c + G \geq O(1)$
(2)	$\Omega_{l_1} + \Omega_{l_2} - \Omega_{l_3} - \tilde{\omega}_{l_4} = 0 \geq G + \Delta \geq O(1)$
(3)	$\Omega_{l_1} - \Omega_{l_2} - \Omega_{l_3} - \tilde{\omega}_{l_4} \geq G - \Delta \geq O(1)$
(4)	$\Omega_{l_1} + \Omega_{l_2} - \tilde{\omega}_{l_3} - \Omega_{l_4} \geq G - \Delta \geq O(1)$
(5)	$ \Omega_{l_1} - \Omega_{l_2} - \tilde{\omega}_{l_3} - \Omega_{l_4} \geq G - \Delta \geq O(1)$
(6)	$ \Omega_{l_1} - \tilde{\omega}_{l_2} - \Omega_{l_3} - \Omega_{l_4} \geq G - \Delta \geq O(1)$

Proposition 2. We can define a symplectic change of coordinates to new variables $a = f(\tilde{a}), a = \tilde{a} + \text{cubic terms}, a = (a_2, \dots, a_N)$ (new variables), $\tilde{a} = (\tilde{a}_2, \dots, \tilde{a}_N)$ (original variables), that is generated by a function \mathcal{S} as in (3.7) that is the sum of monomials $\mathcal{S}_{\mathcal{M}}$ of the form (3.12) with $\sum_{i=1}^4 \sigma(k_j) \omega_{k_i} \geq O(1)$, and that satisfies that

- (i) the subspace V_+ defined by $a_j = 0, \forall j \in \mathcal{I}_-$, is invariant under the Hamiltonian flow of the quartic normal form $\tilde{\mathcal{H}}$ of (3.10), and
- (ii) the quartic Hamiltonian $\tilde{\mathcal{H}}(a)$, restricted to V_+ , is invariant under the action $a_j \mapsto a_j e^{i\phi}$, for all $j \in \mathcal{I}_+, \phi \in \mathbb{R}$.

Proof. To show (i), we consider Hamilton’s equations for $\dot{a}_k, k \in \mathcal{I}_-$. We have

$$\begin{aligned} \dot{a}_k = & -i\omega_k a_k - i \frac{k_4}{4} \left\{ \sum_{k_1, k_2, k_3=2}^N \tilde{\Gamma}_{k_1 k_2 k_3 k} \left(4a_{k_1} a_{k_2} a_{k_3} \right. \right. \\ & + 6a_{k_1} a_{k_2} a_{k_3}^* + 4a_{k_1} a_{k_2}^* a_{k_3}^* \left. \right) \\ & + \sum_{k_1, k_2, k_4=2}^N \tilde{\Gamma}_{k_1 k_2 k k_4} \left(6a_{k_1} a_{k_2} a_{k_4}^* + 4a_{k_1} a_{k_2}^* a_{k_4}^* \right) \\ & + \sum_{k_1, k_3, k_4=2}^N \tilde{\Gamma}_{k_1 k k_3 k_4} 4a_{k_1} a_{k_3}^* a_{k_4}^* \\ & \left. + 4 \sum_{k_2, k_3, k_4=2}^N \tilde{\Gamma}_{k k_2 k_3 k_4} a_{k_2}^* a_{k_3}^* a_{k_4}^* \right\}. \end{aligned} \quad (3.16)$$

To have a solution $a_k(t) = 0$, for all $t, k \in \mathcal{I}_-$, it is sufficient to eliminate monomials $b_{k_1} b_{k_2} b_{k_3}$ with $b_{k_j} = a_{k_j}$ or $b_{k_j} = a_{k_j}^*$ and $k_1, k_2, k_3 \in \mathcal{I}_+$. These monomials come from the monomials of \mathcal{H} shown in Table 2. By (3.13), (3.14), these monomials have frequency sum denominators that are of $O(1)$. This is shown in Table 3, where we use the notation $\Omega_l = \omega_l$, if $l \in \mathcal{I}_+$, and $\tilde{\omega}_l = \omega_l$, if $l \in \mathcal{I}_-$.

Part (ii) follows from the fact that we can eliminate from \mathcal{H} all monomials $a_{l_1} a_{l_2} a_{l_3} a_{l_4}^*, a_{l_1} a_{l_2} a_{l_3} a_{l_4}$, with $l_1, l_2, l_3, l_4 \in \mathcal{I}_+$, and their complex conjugates. The absolute value of the frequency denominator for the monomial $a_{l_1} a_{l_2} a_{l_3} a_{l_4}^*, l_1, l_2, l_3, l_4 \in \mathcal{I}_+$, and its complex conjugate, is by (3.15)

$$\Omega_{l_1} + \Omega_{l_2} + \Omega_{l_3} - \Omega_{l_4} \geq 2\Omega_c - \Delta \geq O(1). \quad (3.17)$$

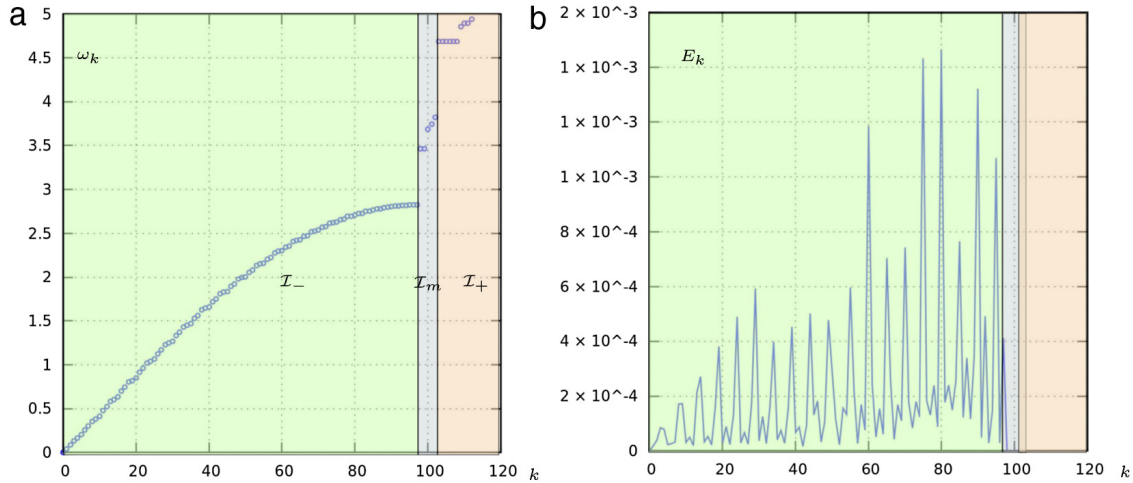


Fig. 11. (a) Dispersion relation of Example 2 and decomposition into low, medium, and high modes, $\mathcal{I}_-, \mathcal{I}_m, \mathcal{I}_+$ respectively. (b) E_k with $k \in \{2, \dots, 103\}$ and $k_2, k_3, k_4 \in \{104, \dots, 113\}$.

Similarly the absolute value of the denominator for $a_{l_1} a_{l_2} a_{l_3} a_{l_4}$, $l_1, l_2, l_3, l_4 \in \mathcal{I}_+$, and its complex conjugate, is by (3.15)

$$\Omega_{l_1} + \Omega_{l_2} + \Omega_{l_3} + \Omega_{l_4} \geq 4\Omega_c \geq O(1). \quad (3.18)$$

Therefore $\tilde{\mathcal{H}}$, restricted to V_+ , and denoted by $\tilde{\mathcal{H}}_+$, is by

$$\tilde{\mathcal{H}}_+(a) = \sum_{l \in \mathcal{I}_+} \omega_l a_l a_l^* + \frac{3k_4}{2} \sum_{l_1, l_2, l_3, l_4 \in \mathcal{I}_+} \tilde{\Gamma}_{l_1 l_2 l_3 l_4} a_{l_1} a_{l_2} a_{l_3}^* a_{l_4}^*. \quad (3.19)$$

By (3.19) we have $\tilde{\mathcal{H}}_+(ae^{i\phi}) = \tilde{\mathcal{H}}_+(a)$, for all $a \in V_+, \phi \in \mathbb{R}$. □

The symmetry under “global phase” change in Proposition 2 (ii) implies that the Hamiltonian flow of $\tilde{\mathcal{H}}_+$ has the additional constant of motion $\mathcal{P}_+ = \sum_{l \in \mathcal{I}_+} |a_l|^2$.

Let \mathcal{O} denote the set of points on such an orbit of the Hamiltonian flow of $\tilde{\mathcal{H}}$ in V_+ . If the modes of \mathcal{I}_+ are spatially localized in the sense of Section 2, the set $f_1(\mathcal{O})$, see the notation of Section 3.1, will also be a spatially localized set, provided that f_1 is sufficiently close to the identity (localization can be measured by distance from the span of the modes of \mathcal{I}_+). We would also need to check that \mathcal{O} is close to an orbit of the full system of (3.9) for a long time. Following the comments on the theory of normal forms in Section 3.1, both assumptions are satisfied as \mathcal{O} is sufficiently close to the origin. Thus localization is seen (at least) in the limit of small amplitude oscillations.

It is a problem for further work to give an estimate of the neighborhood of the origin where \mathcal{O} is a good approximation of a spatially localized solution of the FPU system. Proposition 2, (2.14), and (2.19) imply that the coefficients of the monomials \mathcal{S} are of $O(1)$, i.e. independent of the size of the lattice. This fact can be used to give a rough estimate of \mathcal{S} , see Section 5.

3.3. Invariant subspaces: cases without frequency gaps

In the examples where the gap separating low and high frequency modes becomes smaller (Examples 2, 3), or is absent (Example 4), the bounds on the frequency sums of Table 3 leading to part (i) of Proposition 2 are not possible. For instance, in Example 3 we have a gap around $l = 97$, but its size G is comparable to the width Δ of the high frequency modes above it, and the frequency sum denominators from cases (2)–(6) in Table 3 cannot be readily controlled. In Example 4 we see no frequency gaps, and the argument leading to Proposition 2 seems irrelevant.

The observation of localized modes with small overlap in Examples 2, 3 suggests that the numerators $\tilde{\Gamma}_{k_1 k_2 k_3 k_4}$ in (3.12)

can be small when we are close to some resonances, so that the coefficient of $\mathcal{S}_{\mathcal{M}}$ remains small.

To examine this scenario we decompose the set of frequencies in three sets of “low”, “medium”, and “high” frequency modes, with respective index sets $\mathcal{I}_-, \mathcal{I}_m, \mathcal{I}_+$, see e.g. Fig. 11(a). The sets $\mathcal{I}_-, \mathcal{I}_m, \mathcal{I}_+$ are mutually disjoint, with $\mathcal{I}_- \cup \mathcal{I}_m \cup \mathcal{I}_+ = \{2, \dots, N\}$. Also $i \in \mathcal{I}_-, j \in \mathcal{I}_m$ implies $i < j$, and $j \in \mathcal{I}_m, k \in \mathcal{I}_+$ implies $j < k$.

Given such a decomposition we define E_k by

$$E_k = \max_{k_2, k_3, k_4 \in \mathcal{I}_+} \left\{ \max_{\sigma(j) = \pm 1} \left| \frac{\tilde{\Gamma}_{kk_2 k_3 k_4}}{\sum_{j=1}^4 \sigma(k_j) \omega_{k_j}} \right| \right\}, \quad k \in \mathcal{I}_- \cup \mathcal{I}_m. \quad (3.20)$$

We also define \tilde{E} as

$$\tilde{E} = \max_{k \in \mathcal{I}_- \cup \mathcal{I}_m} \{E_k\}. \quad (3.21)$$

In (3.20) note that the coefficients $\tilde{\Gamma}_{kk_2 k_3 k_4}$ are invariant under permutations of the subindices. Also, $\max_{\sigma(j) = \pm 1}$ denotes maximum over all combinations of the signs $\sigma(j)$ in the frequency sum.

The decomposition into low, medium, and high modes is clearly arbitrary. In Examples 2, 3 the dispersion relation (Figs. 5, 7(a) respectively) shows a jump after the mode where it becomes almost flat; this point is taken as the upper limit of \mathcal{I}_- . In Example 4, the general idea is more speculative, and relies on the existence of spatially localized modes in the highest frequencies, see Fig. 9. We examine various choices of $\mathcal{I}_-, \mathcal{I}_m, \mathcal{I}_+$ so that the E_k , and \tilde{E} remain under some value we choose. At the same time we want the modes in \mathcal{I}_+ to have spatial localization in the sense of Section 2.3.

Also, part (ii) of Proposition 2 requires some control of the frequencies in \mathcal{I}_+ , as in (3.17), (3.18). It will be sufficient to keep $\Omega_c > \Delta$, using Ω_c, Δ as in (3.13), (3.14) but with the present definition of \mathcal{I}_+ .

Example 2. For this example the choice of $\mathcal{I}_-, \mathcal{I}_m$ and \mathcal{I}_+ is suggested by the dispersion relation, see Fig. 11(a). We use $\mathcal{I}_- = \{2, \dots, 98\}$, $\mathcal{I}_m = \{99, \dots, 103\}$, and $\mathcal{I}_+ = \{104, \dots, 113\}$. Fig. 11(b) shows E_k as a function of $k \in \mathcal{I}_- \cup \mathcal{I}_m$ with $k_2, k_3, k_4 \in \mathcal{I}_+$. The plot is divided into three regions, each one representing k in $\mathcal{I}_-, \mathcal{I}_m$ and \mathcal{I}_+ respectively. The first region shows the interaction coefficients between modes in \mathcal{I}_- and modes in \mathcal{I}_+ ; this interaction yields $E_k \leq 10^{-3}$ for all $k \in \mathcal{I}_-$. The second region (the more narrow band) indicates the interaction between modes

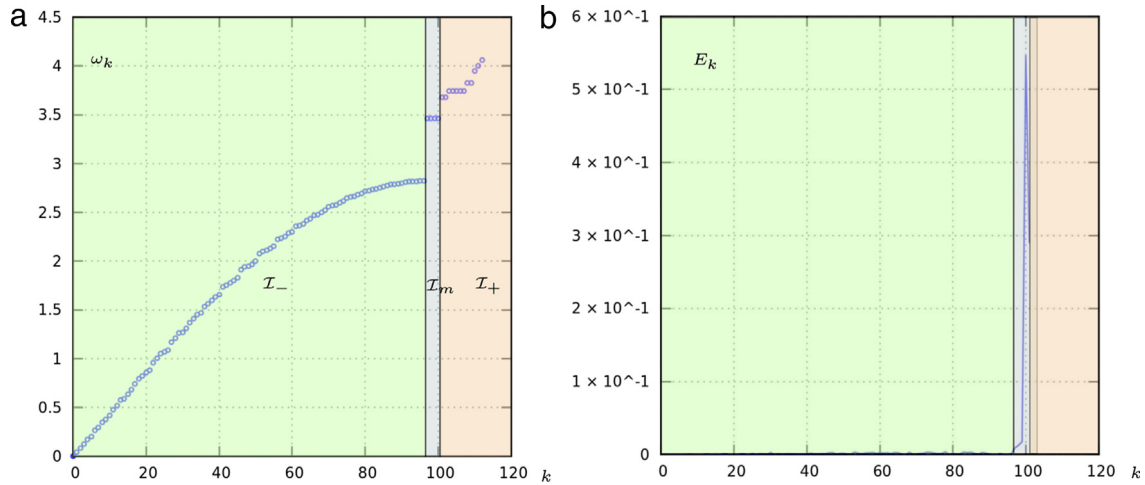


Fig. 12. (a) Dispersion relation of Example 3 and decomposition into low, medium, and high modes, \mathcal{I}_- , \mathcal{I}_m , \mathcal{I}_+ respectively. (b) E_k with $k \in \{2, \dots, 101\}$ and $k_2, k_3, k_4 \in \{102, \dots, 113\}$. E_k is negligible for $k \in \mathcal{I}_-$, larger values are seen for $k \in \mathcal{I}_m$.

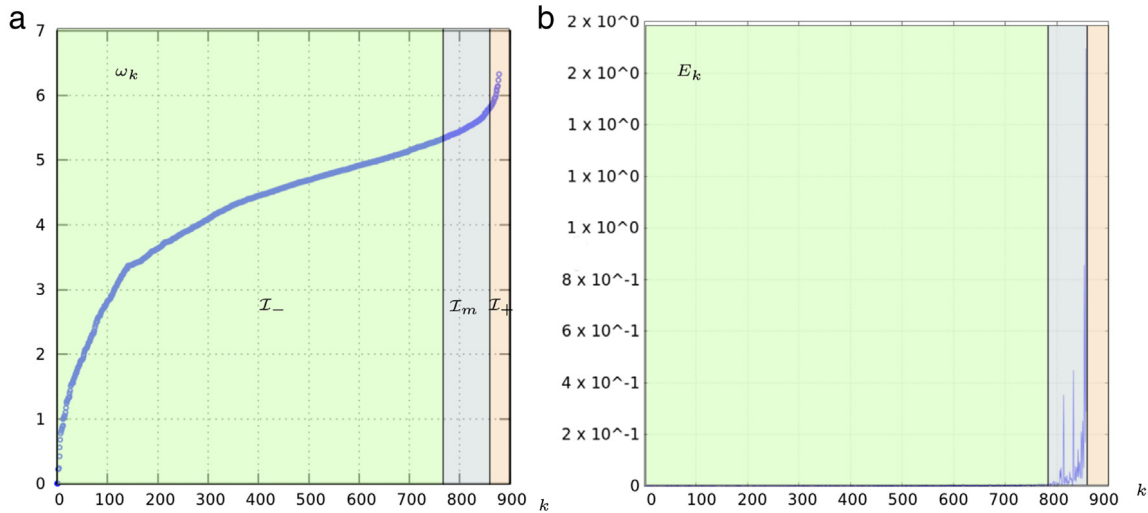


Fig. 13. (a) Dispersion relation of Example 4 and decomposition into low, medium, and high modes, \mathcal{I}_- , \mathcal{I}_m , \mathcal{I}_+ respectively. (b) E_k with $k \in \{2, \dots, 849\}$ and $k_2, k_3, k_4 \in \{850, \dots, 879\}$. E_k is negligible for $k \in \mathcal{I}_-$, larger values are seen for $k \in \mathcal{I}_m$.

in \mathcal{I}_m and modes in \mathcal{I}_+ ; this interaction yields $E_k \leq 10^{-8}$ for all $k \in \mathcal{I}_m$. The third part of the plot is empty since we want $k \in \mathcal{I}_- \cup \mathcal{I}_m$. Thus $\tilde{E} < 10^{-3}$.

Example 3. For this example the criterion for selecting \mathcal{I}_- , \mathcal{I}_m and \mathcal{I}_+ is also suggested by the dispersion relation, see Fig. 12(a). We use $\mathcal{I}_- = \{2, \dots, 97\}$, $\mathcal{I}_m = \{98, \dots, 101\}$, and $\mathcal{I}_+ = \{102, \dots, 113\}$. Fig. 12(b) shows E_k as a function of $k \in \mathcal{I}_- \cup \mathcal{I}_m$ and $k_2, k_3, k_4 \in \mathcal{I}_+$. The plot also is divided in three regions.

The first region indicates the size of the interaction between modes in \mathcal{I}_- and modes in \mathcal{I}_+ ; this interaction yields $E_k \leq 10^{-3}$ for all $k \in \mathcal{I}_-$. The second region (the more narrow band) plots the interaction between modes in \mathcal{I}_m and modes in \mathcal{I}_+ ; the interaction yields $E_k \leq 10^{-1}$ for all $k \in \mathcal{I}_m$, i.e. the peak in Fig. 12 reflects a larger interaction between medium and high modes. The third part of the plot is empty since we want $k \in \mathcal{I}_- \cup \mathcal{I}_m$. Thus $\tilde{E} \leq 10^{-1}$.

Example 4. In this example it is not obvious how to divide the modes of Fig. 13(a). One possible way is to look for k which changes E_k abruptly. For instance, consider k in the interval $\{2, \dots, 849\}$, and $k_2, k_3, k_4 \in \{850, \dots, 879\}$. Fig. 13(b) shows that E_k remains less than 10^{-1} when $k \leq 787$, and starts to grow just passing this value. This indicates that we have left \mathcal{I}_- and are in the range

of modes in \mathcal{I}_m . The interaction continues to increase, reaching $E_k = 10^0$ when we consider $k = 850$. We then choose $\mathcal{I}_- = \{2, \dots, 787\}$, $\mathcal{I}_m = \{788, \dots, 849\}$, and $\mathcal{I}_+ = \{850, \dots, 879\}$, and obtain $\tilde{E} < 10^0$.

We see below that the use of the sets \mathcal{I}_- , \mathcal{I}_m , \mathcal{I}_+ is a device to pass from the frequency gap case to the case without gap, i.e. the size of E_k , $k \in \mathcal{I}_-$ is controlled by the frequency gap, while E_k , $k \in \mathcal{I}_m$, also depends on the coefficients of mode interactions. In what follows however, we use the decomposition into $\mathcal{I}_- \cup \mathcal{I}_m$, and \mathcal{I}_+ and there is no distinction between modes in \mathcal{I}_- or \mathcal{I}_m .

The invariant subspace statement for the quartic normal form is as follows.

Proposition 3. There exists a symplectic change to new variables $a = f(\tilde{a})$, where $a = \tilde{a} + \text{cubic terms (new variables)}$, and $a = (a_{2,1}, \dots, a_{N,D})$, $\tilde{a} = (\tilde{a}_{1,1}, \dots, \tilde{a}_{N,D})$ (old variables), that is generated by a function \mathcal{S} as in (3.7) that is the sum of monomials $\mathcal{S}_{\mathcal{M}}$ of the form (3.12), and with coefficients satisfying either

$$\frac{\tilde{\Gamma}_{k_1 k_2 k_3 k_4}}{\sum_{j=1}^4 \sigma(k_j) \omega_j} \leq \tilde{E},$$

- or $\sum_{j=1}^4 \sigma(k_j)\omega_j \geq 2\Omega_c - \Delta$, Ω_c, Δ as in (3.13), (3.14), such that
- (i) the subspace V_+ defined by $a_{j,d} = 0$, for all $j \in \mathcal{J}_- \cup \mathcal{J}_m$, and $d \in \{1, \dots, D\}$, is invariant under the Hamiltonian flow of the quartic normal form $\tilde{\mathcal{H}}$ of (3.10), and
 - (ii) the quartic Hamiltonian $\tilde{\mathcal{H}}(a)$, restricted to V_+ , is invariant under the action $a_{j,d} \mapsto a_{j,d}e^{i\phi}$, for all $j \in \mathcal{J}_+, d \in \{1, \dots, D\}$, and $\phi \in \mathbb{R}$.

Proof. To see (i) we write the equations for $\dot{a}_{l,d}$, $l \in \mathcal{J}_- \cup \mathcal{J}_m$, as

$$\dot{a}_{l,d} = -i\omega_l a_{l,d} + M_+^l + M_{-/m/+}^l,$$

$$l \in \mathcal{J}_- \cup \mathcal{J}_+, d \in \{1, \dots, D\}, \tag{3.22}$$

where M_+^l represents the sum of monomials of $a_{l,d}, a_{l,d}^*$ with subscript l only in \mathcal{J}_+ , and $M_{-/m/+}^l$ represents the remaining terms. A monomial in M_+^l corresponds to a monomial of \mathcal{H}_4 with coefficient $\tilde{\Gamma}_{lk_2k_3k_4}$, $l \in \mathcal{J}_- \cup \mathcal{J}_m$. By the assumption

$$\frac{\tilde{\Gamma}_{kk_2k_3k_4}}{\sum_i^4 \sigma(k_i)\omega_{k_i}} \leq E_k \leq \tilde{E},$$

all monomials of \mathcal{H}_4 leading to M_+^l can be removed using a symplectic transformation with the properties of the statement.

For part (ii) we eliminate from \mathcal{H} all monomials $a_{l_1,d_1}a_{l_2,d_1}a_{l_3,d_2}a_{l_4,d_2}^*$, $a_{l_1,d_1}a_{l_2,d_1}a_{l_3,d_2}a_{l_4,d_2}$, with $l_1, l_2, l_3, l_4 \in \mathcal{J}_+, d_1, d_2 \in \{1, \dots, D\}$, and their complex conjugates. The coefficient of the monomial \mathcal{S}_M needed to eliminate $a_{l_1,d_1}a_{l_2,d_1}a_{l_3,d_2}a_{l_4,d_2}^*$, $l_1, l_2, l_3, l_4 \in \mathcal{J}_+$ (and its complex conjugate) is

$$\frac{\tilde{\Gamma}_{l_1l_2l_3l_4}}{\sum_{j=1}^4 \sigma(k_j)\omega_{k_j}},$$

with $\left| \sum_{j=1}^4 \sigma(k_j)\omega_{k_j} \right| = \Omega_{l_1} + \Omega_{l_2} + \Omega_{l_3} - \Omega_{l_4} \geq 2\Omega_c - \Delta$.

Similarly, the coefficient of the monomial \mathcal{S}_M needed to eliminate $a_{l_1,d_1}a_{l_2,d_1}a_{l_3,d_2}a_{l_4,d_2}$, $l_1, l_2, l_3, l_4 \in \mathcal{J}_+, d_1, d_2 \in \{1, \dots, D\}$, and its complex conjugate, is

$$\frac{\tilde{\Gamma}_{l_1l_2l_3l_4}}{\sum_{j=1}^4 \sigma(k_j)\omega_{k_j}}, \quad \text{with } \left| \sum_{j=1}^4 \sigma(k_j)\omega_{k_j} \right| = \Omega_{l_1} + \Omega_{l_2} + \Omega_{l_3} + \Omega_{l_4} \geq 4\Omega_c \geq 2\Omega_c - \Delta.$$

Therefore $\tilde{\mathcal{H}}$, restricted to V_+ , and denoted by $\tilde{\mathcal{H}}_+$, is

$$\begin{aligned} \tilde{\mathcal{H}}_+(a) &= \sum_{d=1}^D \sum_{l \in \mathcal{J}_+} \omega_l a_{l,d} a_{l,d}^* \\ &+ \frac{3k_4}{2} \sum_{d_1, d_2=1}^D \sum_{l_1, l_2, l_3, l_4 \in \mathcal{J}_+} \tilde{\Gamma}_{l_1l_2l_3l_4} \\ &\times \left[a_{l_1,d_1} a_{l_2,d_1} a_{l_3,d_2} a_{l_4,d_2}^* \right], \end{aligned} \tag{3.23}$$

and has the desired global phase symmetry. \square

The symmetry under global phase transform in Proposition 3(ii) implies that the Hamiltonian flow of $\tilde{\mathcal{H}}_+$ has the additional constant of motion

$$\mathcal{P} = \sum_{d=1}^D \sum_{k \in \mathcal{J}_+} |a_{k,d}|^2. \tag{3.24}$$

In Section 5 we compute some periodic of orbits of $\tilde{\mathcal{H}}$ in V_+ . Spatial localization for these orbits is as discussed in Section 3.2.

In particular, spatial localization is obtained (at least) in the limit of vanishing amplitudes, assuming that the modes in \mathcal{J}_+ are also spatially localized. The number \tilde{E} can be used to estimate the size of \mathcal{S} , and we expect that smaller \tilde{E} implies that the normal form is a good approximation for larger amplitudes.

4. Periodic orbits in the subspace V_+ and their stability

In this section we compute some periodic solutions of the Hamiltonian flow of $\tilde{\mathcal{H}}_+$ in V_+ . By Propositions 2, 3, these solutions are automatically periodic orbits of the Hamiltonian flow of the quartic normal form $\tilde{\mathcal{H}}$.

We will examine solutions of the Hamiltonian system of $\tilde{\mathcal{H}}_+$ of the form $a = e^{-i\lambda t}A$, $A \in V_+ = \mathbb{C}^{D|\mathcal{J}_+|}$, $\lambda \in \mathbb{R}$. These periodic solutions are often called (discrete) “breathers”, see [6], while A is referred to as the breather amplitude. Discrete breather solutions have been studied extensively in the context of discrete nonlinear Schrödinger equations, see [7].

The breather amplitudes $A \in \mathbb{C}^{D|\mathcal{J}_+|} \approx \mathbb{R}^{2D|\mathcal{J}_+|}$ are also critical points of the Hamiltonian $\tilde{\mathcal{H}}_+(A)$ on the hyperspheres S_c of radius \sqrt{c} in $\mathbb{R}^{2D|\mathcal{J}_+|}$, i.e. $S_c = \{v \in V_+ : \mathcal{P}(v) = c\}$, see e.g. [31]. This implies that there exist at least two such A for each $c > 0$, corresponding to the maximum and minimum of $\tilde{\mathcal{H}}_+$ on S_c . It is a topological fact, see e.g. [17, 18], that we have at least $D|\mathcal{J}_+|$ families (circles) of such critical points A for each sphere S_c (note that A a breather amplitude implies that $e^{i\phi}A$ also is a breather amplitude, for any real ϕ).

To find the maxima (minima) of $\tilde{\mathcal{H}}_+$ on the hypersphere S_c numerically we use the following: we integrate numerically the gradient of $\tilde{\mathcal{H}}_+(-\tilde{\mathcal{H}}_+)$ in $\mathbb{R}^{2D|\mathcal{J}_+|}$ from $t = 0$ to $t = \Delta t$ using an initial condition $\tilde{u}(0)$ on S_c to obtain $u(\Delta t)$. We then rescale to define $\tilde{u}(\Delta t) = [\sqrt{c}/\sqrt{\mathcal{P}(u(\Delta t))}]u(\Delta t)$, and iterate the integration and rescaling steps. (The integration step used a fourth order Runge–Kutta method.) The gradient flow does not preserve \mathcal{P} , but the rescaled iterates $\tilde{u}(n\Delta t)$, $n = 1, 2, \dots$, remain on S_c . For Δt sufficiently small the iterates are expected to converge to local maxima (minima) of $\tilde{\mathcal{H}}_+$ on S_c . These are critical points of $\tilde{\mathcal{H}}_+$ on S_c and must therefore be amplitudes A of a breather solution.

To compute the frequency λ , we use the fact that by $a_{k,d} = e^{i\lambda t}A_{k,d}$, $k \in \mathcal{J}_+$, and (3.23), A, λ satisfy

$$\begin{aligned} \lambda A_{k,d} &= \omega_k A_{k,d} \\ &+ \frac{3k_4}{2} \sum_{d_1, d_2=1}^D \left[\sum_{k_1, k_2, k_4 \in \mathcal{J}_+} \tilde{\Gamma}_{k_1k_2kk_4} A_{k_1,d_1} A_{k_2,d_1} A_{k_4,d_2}^* \right. \\ &\left. + \sum_{k_1, k_2, k_3 \in \mathcal{J}_+} \tilde{\Gamma}_{k_1k_2k_3k} A_{k_1,d_1} A_{k_2,d_1} A_{k_3,d_2}^* \right], \end{aligned}$$

$$\forall k \in \mathcal{J}_+, d \in \{1, \dots, D\}. \tag{4.1}$$

Multiplying by $A_{k,d}^*$ and summing over $k \in \mathcal{J}_+, d \in \{1, \dots, D\}$, we obtain λ in terms of the computed breather amplitude A .

In Fig. 14 we show the evolution of the value of $\tilde{\mathcal{H}}_+$ under this gradient algorithm with rescaling for Example 2. E_{\max}, E_{\min} denote the maximum and minimum respectively of $\tilde{\mathcal{H}}_+(A)$ on S_c .

The system of equations (4.1), with $\mathcal{P} = c$, can be also solved numerically for A and λ using variants of Newton’s method. This more general approach can be used for all critical points, not just local extrema of $\tilde{\mathcal{H}}_+(A)$ on S_c , see e.g. [32].

In Figs. 15–17 we show some results of the gradient algorithm above for Examples 2, 3, and 4.

Figs. 15, 16 correspond to Examples 2, 3 respectively and show the amplitudes for the minimizer of $\tilde{\mathcal{H}}_+$ on the hypersphere S_c . We used $c = 0.0022, 0.28$ respectively, and see that in both cases the amplitude is strongly concentrated at the lowest mode of \mathcal{J}_+ . In the 3-D example of Fig. 17 we see that the amplitude is spread among

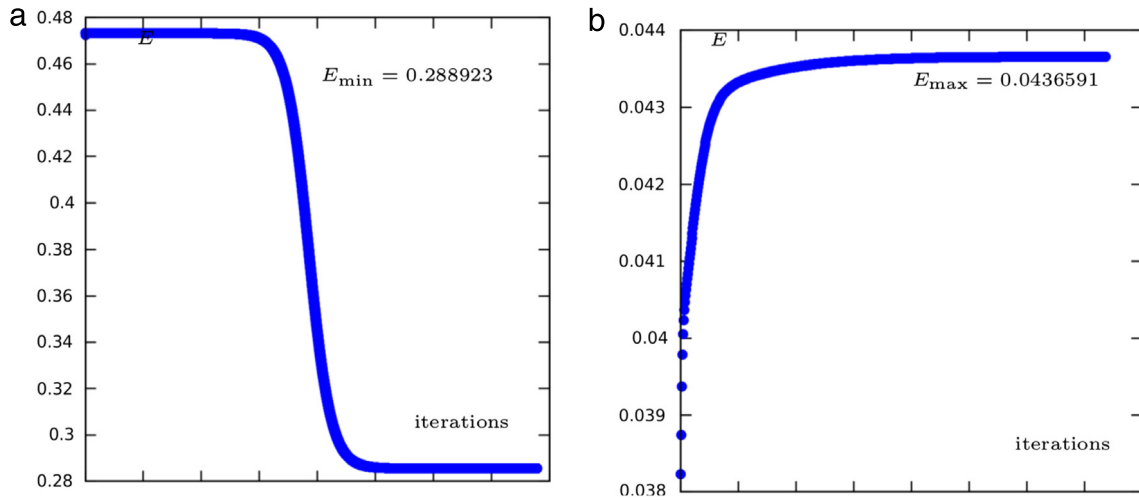


Fig. 14. Evolution of E (value of $\tilde{\mathcal{H}}_+$) under gradient flow with rescaling of $\tilde{\mathcal{H}}_+$ of Example 2, (a) gradient flow with rescaling of $-\tilde{\mathcal{H}}_+$, (b) gradient flow with rescaling of $\tilde{\mathcal{H}}_+$. We used $k_2 = 1, k_4 = 1, \mathcal{I}_+ = \{99, \dots, 109\}, \mathcal{P} = 0.0022$.

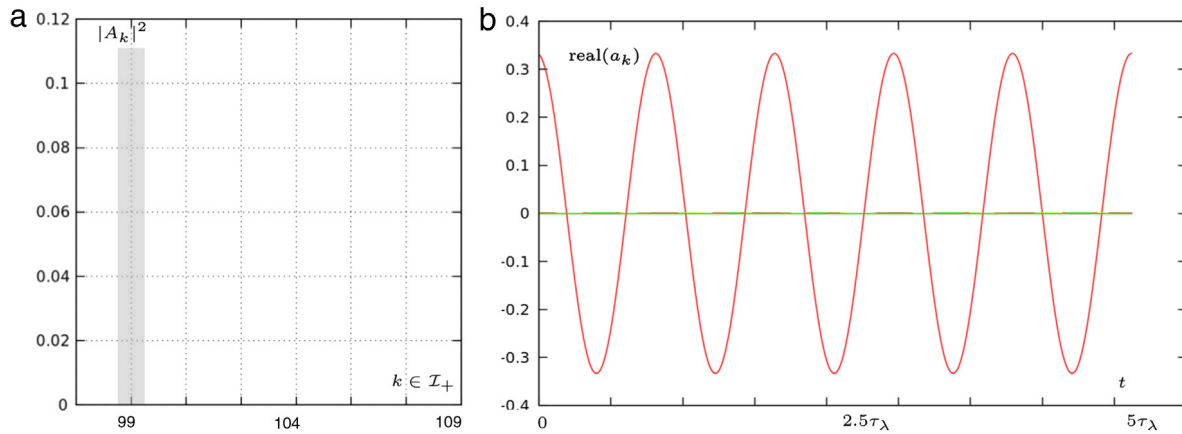


Fig. 15. Example 2: (a) $|A_k|^2$ vs. $k \in \mathcal{I}_+$ for breather amplitude A computed by gradient (descent) method with rescaling, $k_2 = 1, k_4 = 1, \mathcal{P} = 0.0022$. The amplitude is concentrated in the lowest mode. (b) Real part of $a_k(t)$ vs. time $t, k \in \mathcal{I}_+, a(t)$ numerical solution of Hamilton's equations for $\tilde{\mathcal{H}}_+$, using as initial condition the breather amplitude A computed in (a).

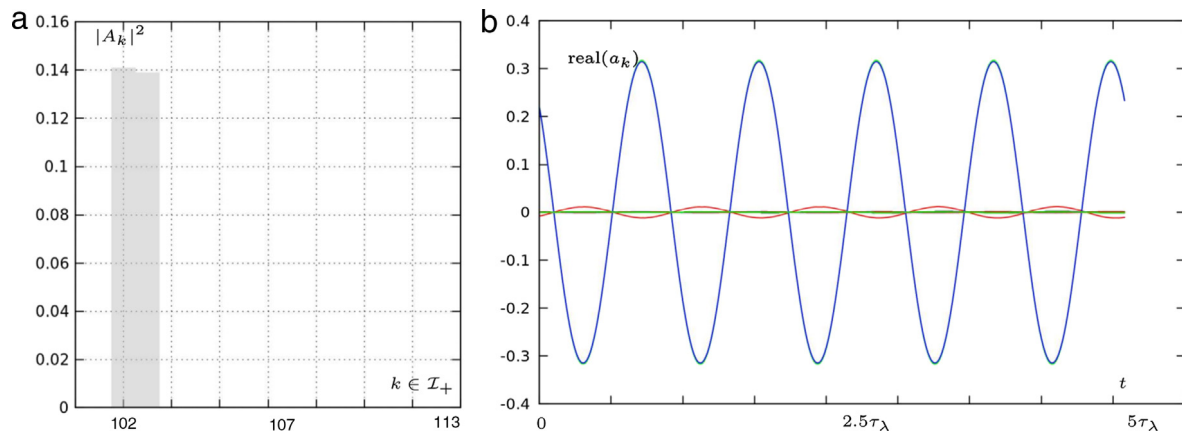


Fig. 16. Example 3: (a) $|A_k|^2$ vs. $k \in \mathcal{I}_+$ for breather amplitude A computed by gradient (descent) method with rescaling, $k_2 = 1, k_4 = 1, \mathcal{P} = 0.28$. The amplitude is concentrated in the lowest mode. (b) Real part of $a_k(t)$ vs. time $t, k \in \mathcal{I}_+, a(t)$ numerical solution of Hamilton's equations for $\tilde{\mathcal{H}}_+$ in V_+ , using as initial condition the breather amplitude A computed in (a).

several modes. ($A_{k,d}$ depends on the component index d , we only show $d = 1$.)

To verify that the amplitudes A computed by the gradient algorithm are indeed amplitudes of breather solutions, we integrate numerically Hamilton's equations for each $\tilde{\mathcal{H}}_+$ using a

fourth order Runge–Kutta method. Figs. 15–17(b) indicate that the amplitudes of the modes of \mathcal{I}_+ oscillate with constant amplitude.

The solutions computed are continuations of the normal mode solutions of the $k_4 = 0$ (i.e. linear) problem. This is verified numerically by computing the solutions with smaller values of k_4 .

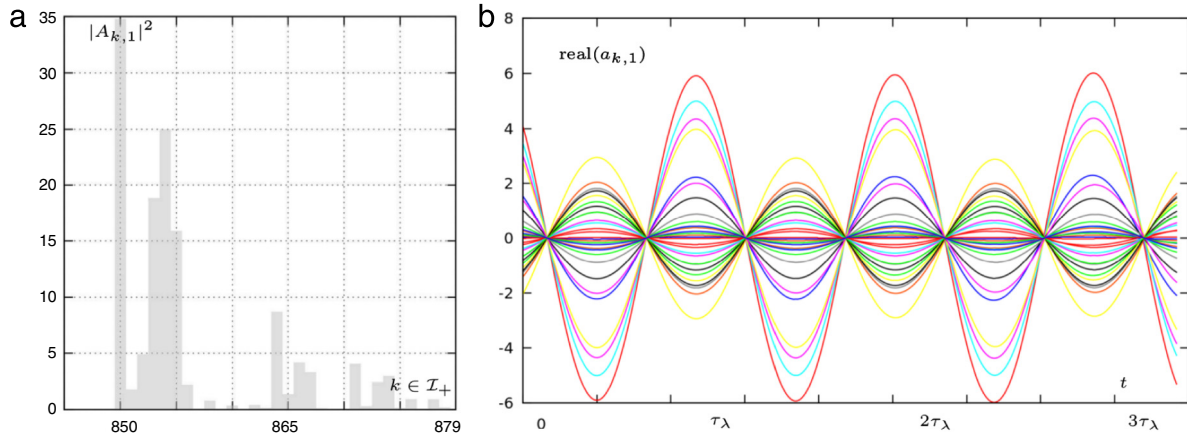


Fig. 17. Example 4: (a) Distribution of the amplitudes $|A_{k,1}|^2$ vs. $k \in \mathcal{I}_+$, for the breather amplitude A computed by the gradient (descent) method with rescaling, $k_2 = 1$, $k_4 = 1$, $\mathcal{P} = 85.50$. (b) Real part of $a_k(t)$ vs. time t , $k \in \mathcal{I}_+$, $a(t)$ numerical solution of Hamilton's equations for $\tilde{\mathcal{H}}_+$ in V_+ , using as initial condition the breather amplitude A computed in (a).

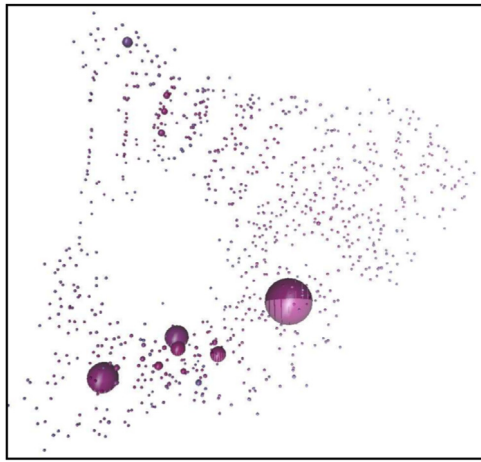


Fig. 18. Amplitudes of breather of Fig. 17, $k_2 = 1$, $k_4 = 1$, $\mathcal{P} = 85.50$. Size of radius at site i is proportional to $|\mathbf{q}_i|$, where \mathbf{q} is obtained from $a_{k,d} = A_{k,d}$, $A_{k,d}$ the computed breather amplitude, via (2.17), (2.12). Amplitudes are concentrated in a small number of sites.

(Equivalently, we can fix k_4 and decrease the hypersphere radius \sqrt{c} .) By (2.18), the minimum and maximum energies of the $k_4 = 0$ system are attained for the lowest and higher frequency modes of \mathcal{I}_+ respectively. The concentration of the amplitude in the lower modes is seen in Fig. 15(a), is due to the fact that we are using the descent algorithm for relatively small values of c . In Example 4, vanishing k_4 makes the amplitude concentrate in the lowest mode. The calculation of Fig. 17 used a relatively large value of c .

By the closing remarks of Subsections 3.1–3.2, spatial localization of the solutions of Figs. 15, 16 is due to the spatial localization of the all the modes of \mathcal{I}_+ , assuming sufficiently small amplitudes. Specifically, by Section 3.2, the lowest modes of \mathcal{I}_+ for the examples of Figs. 15, 16 are $l = 104, 102$ respectively. Spatial localization for these modes is quantified in Section 2.3, see Examples 2, 3. For the 3-D example, Fig. 18, we used the computed breather amplitudes $A_{k,d}$ to obtain the amplitudes of the oscillation in the original displacement variables \mathbf{q} , i.e. \mathbf{q} is obtained from $a_{k,l} = A_{k,d}$, and (2.17), (2.12). Following the comments of Sections 3.1–3.3, this visualization of the spatial shape of the nonlinear normal mode is only guaranteed to be a good approximation in the limit where k_4 or c vanishes. Fig. 17 is nevertheless indicative of the spatial distribution of the amplitudes seen in breather amplitudes obtained for smaller k_4 . The amplitude is always seen to be concentrated in a small subset of the lattice sites, with some shifts of the positions

of largest amplitudes as k_4 is decreased. Our study has included the computation of breathers that maximize the energy, with similar results. In the 3-D case, a breather obtained with $k_4 = 0.2$, $c = 85.5$, has amplitudes that are concentrated in the maximum of the highest frequency linear mode, shown in Fig. 9(b). Thus localization seems even more robust for the maximum energy breather.

To study the linear stability of the computed breather solutions in the subspace V_+ we use the change of variables

$$a_{k,d}(t) = e^{-i\lambda t} b_{k,d}(t), \quad k \in \mathcal{I}_+, d \in \{1, \dots, D\}, \quad (4.2)$$

and Hamilton's equations for $\tilde{\mathcal{H}}_+$ to obtain

$$\begin{aligned} \dot{b}_{k,d} &= i(\lambda - \omega_k) b_{k,d} \\ &- i \frac{3k_4}{2} \sum_{d_1, d_2=1}^D \left[\sum_{k_1, k_2, k_4 \in \mathcal{I}_+} \tilde{\Gamma}_{k_1 k_2 k k_4} b_{k_1, d_1} b_{k_2, d_1} b_{k_4, d_2}^* \right. \\ &\left. + \sum_{k_1, k_2, k_3 \in \mathcal{I}_+} \tilde{\Gamma}_{k_1 k_2 k_3 k} b_{k_1, d_1} b_{k_2, d_1} b_{k_3, d_2}^* \right]. \end{aligned} \quad (4.3)$$

By (4.1), the vector A of the $A_{k,d}$, i.e. the breather amplitude, is a fixed point of (4.3).

The reduction of the stability analysis of a breather orbit to the linear stability analysis of its amplitude is a standard approach for NLS equations, see e.g. [7]. Letting

$$b_{k,d} = A_{k,d} + v_{k,d}, \quad k \in \mathcal{I}_+, d \in \{1, \dots, D\}, \quad (4.4)$$

we have

$$\begin{aligned} \dot{v}_{k,d} &= i(\lambda - \omega_k) v_{k,d} \\ &- i \frac{3k_4}{2} \sum_{d_1, d_2=1}^D \left[\sum_{k_1, k_2, k_4 \in \mathcal{I}_+} \tilde{\Gamma}_{k_1 k_2 k k_4} (v_{k_1, d_1} A_{k_2, d_1} A_{k_4, d_2}^* \right. \\ &+ A_{k_1, d_1} v_{k_2, d_1} A_{k_4, d_2}^* + A_{k_1, d_1} A_{k_2, d_1} v_{k_4, d_2}^*) \\ &+ \sum_{k_1, k_2, k_3 \in \mathcal{I}_+} \tilde{\Gamma}_{k_1 k_2 k_3 k} (v_{k_1, d_1} A_{k_2, d_1} A_{k_3, d_2}^* \\ &+ A_{k_1, d_1} v_{k_2, d_1} A_{k_3, d_2}^* + A_{k_1, d_1} A_{k_2, d_1} v_{k_3, d_2}^*) \left. \right] + O(2), \end{aligned} \quad (4.5)$$

where $O(2)$ means quadratic and higher order terms in $v_{k,d}$ and $v_{k,d}^*$. Letting

$$\begin{aligned} A_{k,d} &= Q_{k,d} + iP_{k,d}, \quad v_{k,d} = q_{k,d} + ip_{k,d}, \\ k &\in \mathcal{I}_+, d \in \{1, \dots, D\}, \end{aligned} \quad (4.6)$$

(4.5) can be also written as

$$\begin{pmatrix} \dot{q} \\ \dot{p} \end{pmatrix} = \begin{pmatrix} \mathbb{O} & \mathbb{I} \\ -\mathbb{I} & \mathbb{O} \end{pmatrix} \begin{pmatrix} \mathcal{A} & \mathcal{B} \\ \mathcal{B} & \mathcal{C} \end{pmatrix} \begin{pmatrix} q \\ p \end{pmatrix}, \quad (4.7)$$

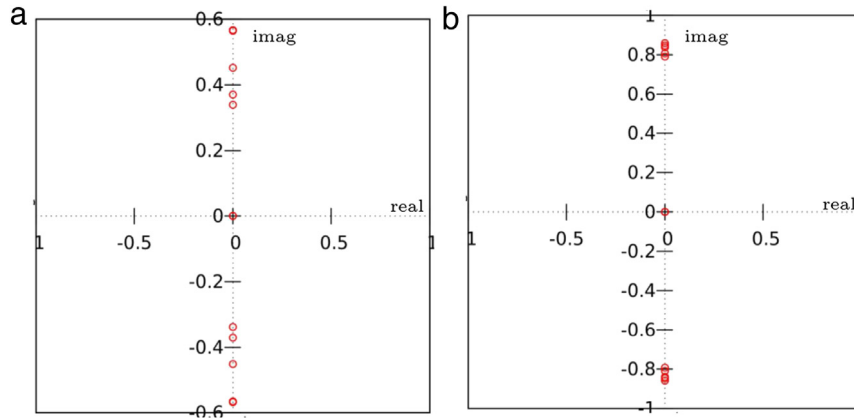


Fig. 19. Eigenvalues in the complex plane for two examples of the matrix (4.7): (a) Example 2, breather of Fig. 15. $k_2 = 1, k_4 = 1,$ and $\mathcal{P} = 0.0022,$ (b) Example 4, breather of Fig. 17. $k_2 = 1, k_4 = 1,$ and $\mathcal{P} = 85.50.$

with $k, l \in \mathcal{I}_+,$ and $q = [q_{1,1}, \dots, q_{N,D}]^T, p = [p_{1,1}, \dots, p_{N,D}]^T.$ The matrices \mathcal{A}, \mathcal{B} and \mathcal{C} are symmetric so that the matrix of the linear system (4.7) is Hamiltonian. They are given by

$$\begin{aligned} \mathcal{A}_{kl} &= (\lambda - \omega_k)\delta_{kl} - 3k_4 \sum_{d_1, d_2=1}^D \sum_{s_1, s_2 \in \mathcal{I}_+} \tilde{\Gamma}_{kls_1s_2} \\ &\quad \times (3Q_{s_1, d_1} Q_{s_2, d_2} + P_{s_1, d_1} P_{s_2, d_2}), \\ \mathcal{B}_{kl} &= 3k_4 \sum_{d_1, d_2=1}^D \sum_{s_1, s_2 \in \mathcal{I}_+} \tilde{\Gamma}_{kls_1s_2} (3Q_{s_2, d_2} P_{s_1, d_1} - Q_{s_1, d_1} P_{s_2, d_2}), \\ \mathcal{C}_{kl} &= (\lambda - \omega_k)\delta_{kl} - 3k_4 \sum_{d_1, d_2=1}^D \sum_{s_1, s_2 \in \mathcal{I}_+} \tilde{\Gamma}_{kls_1s_2} (Q_{s_1, d_1} Q_{s_2, d_2} \\ &\quad + 3P_{s_1, d_1} P_{s_2, d_2}). \end{aligned} \quad (4.8)$$

The eigenvalues of the matrix of (4.7) obtained for the computed breathers of Examples 2–4 are seen to be imaginary, see e.g. Fig. 19. This confirms that the computed breathers are linearly stable in the subspace $V_+.$ Numerical computations used the GLS libraries [26].

Linear stability in the invariant subspaces V_+ does not imply linear stability for the flow of the quartic normal form Hamiltonian $\tilde{\mathcal{H}}$ in the whole phase $\mathbb{C}^N.$ This question is left for further work. Numerical integration of the FPU elastic network system, using as initial conditions the approximate solutions computed here, suggests that most of the amplitude remains in the higher frequency modes over time scales of at least $10^3 \tau_{\max},$ where τ_{\max} is the smallest period of the linear system, using in all cases $k_4 \in [0, 1].$ These results required higher order numerical integrators, and additional checks and will be presented elsewhere.

5. Discussion

We used Birkhoff normal forms to compute approximate periodic orbits of inhomogeneous FPU-type systems. These periodic orbits are also spatially localized at small amplitudes. We have verified that the presence of agglomeration regions leads to spatially localized linear normal mode in three 1-D examples, and we have also seen indications of linear spatial localization in a 3-D model with the geometry of a protein. Thus a linear mode analysis is a reasonable first step for examining spatial localization at the weakly nonlinear regime. The second hypothesis, that certain possible near-resonant interactions between high and medium frequency modes are controlled by the small size of the corresponding interaction coefficients is verified by checking that the ratios E_k, \tilde{E} of Proposition 3 are at most unity for the examples considered. The ratios are smaller for the 1-D examples, where

localization in the high frequency modes is also more pronounced. The results for the 3-D example suggest that the weakly nonlinear localization idea is plausible, that it should be corroborated with further studies. Further examples will be presented in future work.

Our work can be extended in several directions. It would be desirable to have theoretical results on the spectrum and the spatial properties of the linear modes, this seems possible in 1-D examples.

Technical issues related to Birkhoff normal forms will be addressed in future work. An estimate of the radius of convergence ρ of the normal form will give us a quantitative estimate of the maximum amplitude of the oscillations we are considering. To estimate ρ we can use more detailed bounds on the size of the coefficients of (3.12), e.g. a count of the terms in different size ranges instead of the bounds E_k, \tilde{E} of Proposition 3. Normal form ideas to find asymptotic invariants, see [16], could be useful in the question of stability of the solutions considered. Related numerical results will be presented elsewhere.

The Lyapunov center theorem may be directly applicable to some low frequency modes, but seems problematic for high frequency modes, where we see many nearby frequencies. The application of this theory would rely on the numerically computed spectrum, e.g. [8,12] apply the theorem to homogeneous FPU lattices where the frequencies are known exactly.

The present study can be further extended by numerical methods that look for periodic orbits directly. The method of [4] is a Galerkin truncation of the Fourier method, which is in principle applicable for arbitrary amplitudes, see e.g. [33] for recent extensions and more references.

Related high order finite difference methods for Hamiltonian systems with continuation from the origin are described in [34,35]. This approach seems closer to what we would like to accomplish in this work. In particular, it would be desirable to continue small amplitude localized periodic orbits to higher amplitudes.

There is also some additional intuition inherent in the quartic model and in the work of [4] that we do not seem to capture. The idea that we can have localization at regions with more connections is verified numerically at the linear level in our study, and use this fact as the basis for studying the weakly nonlinear problem. Nevertheless, additional “stiffness” in these regions due to the quartic terms may make localization even more robust. We do not have a theoretical scheme at present that could use this idea and relied instead on linear localization, which is tacitly assumed to be more tractable, at least for some examples. We note that there is a large literature where nonlinear localization effects are modeled by on-site anharmonic potentials, see e.g. [36] and references.

Another issue is the applicability of the normal form argument we used in the presence of cubic terms. The existence of invariant

subspaces of modes of nearby frequencies in the quartic normal form can be shown in many contexts, see e.g. [37,38] but requires the elimination of cubic terms. Thus there is a question of how the results on high frequency modes could depend on additional terms. A related question is what terms would be physically interesting, given a more realistic model, see also the discussion of Section 2.1. Some problems of this type could be addressed first in 1-D models.

Acknowledgments

We would like to thank Luis Cisneros Ake, David Sanders, and Manuel Tejada for helpful discussions. This work was partially supported by grant SEP-Conacyt 177246.

References

- [1] B. Juanico, Y.H. Sanejouand, F. Piazza, P. De Los Rios, Discrete breathers in nonlinear network models of proteins, *Phys. Rev. Lett.* 99 (2007) 238104.
- [2] M. Tirion, Large amplitude elastic motions in proteins from a single-parameter, atomic analysis, *Phys. Rev. Lett.* 77 (1996) 1905.
- [3] F. Piazza, Y.H. Sanejouand, Discrete breathers in protein structures, *Phys. Biol.* 5 (2008) 026001.
- [4] F. Piazza, Y.H. Sanejouand, Breather-mediated energy transfer in proteins, *Discrete Contin. Dyn. Syst. S* 4 (2011) 1247–1266.
- [5] F. Martínez-Farías, P. Panayotaros, A. Olvera, Weakly nonlinear localization for a 1-D FPU chain with clustering zones, *Eur. Phys. J.* 223 (2014) 2943–2952.
- [6] J.C. Eilbeck, P.S. Lomdahl, A.C. Scott, The discrete self-trapping equation, *Physica D* 16 (1985) 318–338.
- [7] P.G. Kevrekidis, *The Discrete Nonlinear Schrödinger Equation*, Springer, New York, 2009.
- [8] S. Flach, M.V. Ivanchenko, O.I. Kanakov, q-breathers and the Fermi–Pasta–Ulam problem, *Phys. Rev. Lett.* 95 (2005) 064102.
- [9] C. Antonopoulos, T. Bountis, C. Skokos, Chaotic dynamics of N-degree of freedom Hamiltonian systems, *Internat. J. Bifur. Chaos* 16 (2006) 1777–1793.
- [10] H. Christodoulidi, C. Euthymiopoulos, T. Bountis, Energy localization on q-tori, long term stability and the interpretation of FPU recurrences, *Phys. Rev. E* 81 (2010) 016210.
- [11] H. Christodoulidi, C. Euthymiopoulos, Low-dimensional q-tori in FPU lattices: dynamics and localization properties, *Physica D* 261 (2013) 93–113.
- [12] M.V. Ivanchenko, O.I. Kanakov, K.G. Mishagin, S. Flach, q-breathers in finite two- and three-dimensional nonlinear acoustic lattices, *Phys. Rev. Lett.* 97 (2006) 025505.
- [13] S. Flach, A. Ponno, The Fermi–Pasta–Ulam problem: Periodic orbits, normal forms and resonance overlap criteria, *Physica D* 237 (2007) 908–917.
- [14] D. Bambusi, A. Ponno, On metastability in FPU, *Comm. Math. Phys.* 264 (2006) 539–561.
- [15] A. Henrici, T. Kapeler, Resonant normal form for even periodic FPU chains, *J. Eur. Math. Soc.* 11 (2009) 1025–1056.
- [16] T. Genta, A. Giorgilli, S. Paleari, T. Penati, Packets of resonant modes in the Fermi–Pasta–Ulam system, *Phys. Lett. A* 376 (2012) 2038–2044.
- [17] A. Weinstein, Normal modes for non-linear Hamiltonian systems, *Invent. Math.* 20 (1973) 47–57.
- [18] J. Moser, Periodic orbits near an equilibrium and a theorem by Alan Weinstein, *Comm. Pure Appl. Math.* 29 (1976) 727–747.
- [19] H. Hofer, E. Zehnder, *Symplectic Invariants and Hamiltonian Dynamics*, Birkhäuser, Basel, 1994.
- [20] K. Meyer, G. Hall, *Introduction to Hamiltonian Dynamical Systems and the N-Body Problem*, Springer, New York, 2008.
- [21] D. ben-Avraham, M. Tirion, Dynamic and elastic properties of F-Actin, a normal-modes analysis, *Biophys. J.* 68 (1995) 1231–1245.
- [22] S. Nicolay, Y.H. Sanejouand, Functional modes of proteins are among the most robust, *Phys. Rev. Lett.* 96 (2006) 078104.
- [23] I. Bahar, A.R. Atilgan, R.L. Jernigan, B. Erman, Understanding the recognition of protein structural classes by aminoacid composition, *Proteins: Struct. Funct. Genet.* 29 (1997) 172–185.
- [24] P. Van Mieghem, *Graph Spectra for Complex Networks*, Cambridge University Press, Cambridge, 2011.
- [25] R.G. Littlejohn, K.A. Mitchell, Gauge theory of small vibrations in polyatomic molecules, in: P. Newton, P. Holmes, A. Weinstein (Eds.), *Geometry, Mechanics, and Dynamics*, Springer, New York, 2002.
- [26] M. Galassi, J. Davies, GNU Scientific library reference manual, The GSL Team, 2009. https://www.gnu.org/software/gsl/manual/html_node/.
- [27] W.G. Scott, B. James, Capturing the structure of a catalytic RNA intermediate: the Hammerhead Ribozyme, *Science* 274 (1996) 2065–2069.
- [28] PDB Protein Data Bank, An information portal to biological macromolecular structures, 2015. <ftp://ftp.wwpdb.org>.
- [29] F. Fassó, G. Benettin, Composition of Lie transforms with rigorous estimates and applications to Hamiltonian perturbation theory, *Appl. Math. Phys.* 140 (1989) 307–329.
- [30] E. Valdinoci, Tori di transizione nella teoria KAM, Tesis Laurea Univ. Roma 3 (1998).
- [31] P. Panayotaros, Instabilities of breathers in a finite NLS lattice, *Physica D* 241 (2012) 847–856. D.
- [32] P. Panayotaros, Continuation and bifurcations of breathers in a finite discrete NLS equation, *Discrete Contin. Dyn. Syst. S* 4 (2011) 1227–1245.
- [33] R. Castelli, M. Gameiro, J.P. Lessard, Rigorous numerics for ill-posed PDEs: periodic orbits in the Boussinesq equation, 2015. arXiv:1509.08648.
- [34] E.J. Doedel, W. Govaerts, Y.A. Kuznetsov, Computation of periodic solution bifurcations in ODEs using bordered systems, *SIAM J. Numer. Anal.* 41 (2003) 401–435.
- [35] E.J. Doedel, R.C. Paffenroth, H.B. Keller, D.J. Dichmann, J. Galán-Vioque, A. Vanderbauwhede, Computation of periodic solutions of conservative systems with application to the 3-body problem, *Internat. J. Bifur. Chaos* 13 (2003) 1353–1381.
- [36] D. Bambusi, A. Paleari, T. Penati, Existence and continuous approximations of small amplitude breather in 1D and 2D Klein-Gordon lattices, 2009. arXiv:0909.3467v1.
- [37] R. de la Llave, P. Panayotaros, Gravity waves on the surface of the sphere, *J. Nonlinear Sci.* (1996) 147167.
- [38] P. Panayotaros, Near-monochromatic water waves on the sphere, *Physica D* 130 (1999) 273–290.